Progress towards ultra-cold ensembles of rubidium and lithium

by

Swati Singh

B.Sc., McMaster University, 2004

A THESIS SUBMITTED IN PARTIAL FULFILMENT OF
THE REQUIREMENTS FOR THE DEGREE OF

Master of Science

in

The Faculty of Graduate Studies

(Physics)

The University of British Columbia

April, 2007

Abstract

The work described in this thesis is related to various projects that I worked on towards the production of ultra-cold ensembles of ^{85}Rb, ^{87}Rb and fermionic ^{6}Li. In the past few years, ultra-cold atomic gases have evolved into a mature field of research, driving various theoretical and experimental groups towards new possibilities.

This thesis starts with an overview of the research direction of the field and the lab in particular, to use ultra-cold fermionic atoms as quantum simulators for several condensed matter problems. It discusses the experimental route to quantum degeneracy in a sample of ultra-cold atoms and techniques to get there. The rest of the thesis primarily discusses the first step to degeneracy- production of ultra-cold ensembles of rubidium and lithium. It starts with the theoretical concepts that enable laser cooling and trapping. The interaction between light and atoms and how it leads to a decrease in temperature of the ensemble is discussed. The limits of different cooling mechanism with relevance of the atoms of interest are described. The starting point for all laser cooling experiments is an atomic source, the details of the requirements and efficiency of different atomic sources is discussed, emphasizing our choice of sources for the two atoms. Other technical details such as the vacuum system and the control system for the experiment are briefly discussed. Preliminary data from our first ensembles of ultra-cold lithium and rubidium is shown. At the end, the planning and progress of the first experiments that we aim to achieve with these ultra-cold atoms-namely looking for Feshbach resonances and studying the effect of DC electric fields on them, and studies with ultra-cold lithium atoms in optical lattices, is discussed.

Contents

List of Tables

List of Figures

Acknowledgements

This thesis is a testament to the progress made in our Quantum Degenerate Gases Lab. To claim it as my work would be simply incorrect. I would like to take this opportunity to express my gratitude to the people I have met. First and foremost, I am indebted to Prof. Kirk Madison for giving me the opportunity to work in his group. Kirk has always had the time to answer my innumerable whys, all of which were not confined to the experiment. As I write this section and reflect, I realize how enriching those interactions have been. This thesis would not be what it is if it wasn't for my second reader Prof. John Behr, who turned his comments and suggestions into a scientific discussion at times, for which I am grateful.

I think everyone in the lab can attest to the fact that our lab is completely dysfunctional without Dr. Bruce Klappauf. He comes to our rescue when we are willing to give up and inspires us with his remarkable dedication and knowledge. I have witnessed my fellow graduate students Janelle van Dongen and Keith Ladouceur absorb new ideas and quickly master them. Thanks to Janelle for constantly reminding me to keep faith and helping me with things- I owe her over a hundred cookies. Keith has answered many silly computer control questions patiently and is fun to work with. Thanks to Tao for LaTeX and machining help, and for letting me beat him in arm wrestling.

Our lab has been very fortunate to have dedicated undergrads and exchange students. Sylvain Hermelin and Paul Lebel had to be kicked out at times. Sylvain-tight optics is a lab standard and Paul has been named Magneto because of his work on the magnetic coils. Thanks also to Friedrich, Nina and Bastian for their input on experiments, this thesis and my hopeless German. The machine shop and the electronics shop guys have also been very helpful.

I have been fortunate to have a great support network of friends. Anand, Arvind, Sibyl and JonBen would be remembered for food and stimulating conversations- especially Anand. Thanks also to Sasha for her sanity checks and Thilo for smiles.

Most of all, my immense gratitude goes to my family, especially my mother for either believing in me or giving up on me- whatever it was. Last, but definitely not the least, thanks to Abhyudai, now my husband, for being, according to him, a constant source of distraction during this work. As usual I disagree with him and look forward to both silly and intellectual arguments- and a lot more.

Chapter 1

Introduction

TELL me not, in mournful numbers,
Life is but an empty dream !
For the soul is dead that slumbers,
And things are not what they seem.
Life is real ! Life is earnest!
And the grave is not its goal ;
Dust thou art, to dust returnest,
Was not spoken of the soul.

A Psalm of Life : Henry Wadsworth Longfellow

1.1 Phase space density

Classically, the phase space density of an ensemble $\rho(\overrightarrow{r}, \overrightarrow{p}, t)$ can be defined as the probability that a single particle is at position $\overrightarrow{r}$ and has momentum $\overrightarrow{p}$ at some time t. In classical mechanics it is possible to know simultaneously the position and momentum of a single particle with certainty. These six components span the phase space of the particle. The phase space density for a system of N particles is the sum of the single-particle phase space densities of all the particles in the system divided by N. Since the phase space density is a probability, it is always positive and can be normalized over the $6N$-dimensional phase space spanned by the position and momentum vectors.

The quantum mechanical description of a gas of atoms is that of wave-packets interfering with each other. While is it convenient to picture them as billiard balls at high temperatures, specific quantum effects must be taken into account at lower temperatures, as the wave-packets spread and begin to overlap. The spatial extent of the wave-packet is characterized by its de Broglie wavelength, $\lambda_{dB} = h/p_0$, where p_0 is the average momentum of the particle [25]. For a gas at temperature T, the average velocity is simply

$$v_0 = \sqrt{\frac{3k_B T}{m}} \tag{1.1}$$

which gives us the corresponding wavelength scale:

$$\lambda = \frac{h}{\sqrt{3mk_B T}} \tag{1.2}$$

One must remember that since the spatial and momentum spread must satisfy the uncertainty relation, the above expression for λ is an estimate of the degree of spatial localization.

Now, for an ensemble of atoms to be treated classically, the inter-particle spacing

must be much greater than the spatial extent of the wave-packets. Quantum effects become important when the particles tend to overlap, meaning

$$n\lambda^3 \approx 1 \tag{1.3}$$

(onset of Quantum effects).

Here, n is the number density of the ensemble being considered. Figure 1.1 shows the two regimes. The following table gives us an idea of the density and temperature
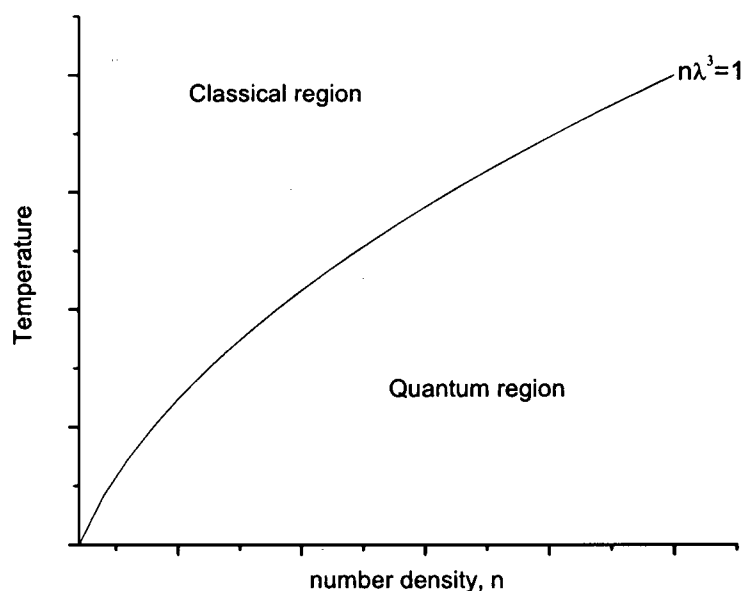
Figure 1.1: Classical and Quantum regimes in the temperature-density space. The rough demarcation between the two is given by $n\lambda^3 = 1$, where λ is the deBroglie wavelength.

values for which quantum degeneracy is achieved in various systems [44]. T_0 is the temperature associated with Equation 1.3. It is important to emphasize here that quantum mechanics is not exclusively the physics of small things, as can be seen in Figure 1.1 and the table below. The quantum mechanical behaviour becomes dominant when the density is high enough so that each particle's wave-function overlaps with its neighbour. The following sections describe briefly how quantum degeneracy is realized in a system of ultra-cold atoms. The tentative approach of our research group is described thereafter.

1.2 Bosons and Fermions- The statistics of identical particles

If two particles are identical, mathematically it means that the Hamiltonian of the two-particle system is invariant under a permutation of their co-ordinates. This leads

Table 1.1: Different systems exhibiting quantum degenerate behaviour.

System	Density (in cm^{-3})	T_0(in K)
Neutron star	10^{37}	10^8
Electrons in metal	10^{22}	10^4
Liquid ^4He	2×10^{22}	2
H_2 gas	2×10^{19}	5×10^{-2}
^{87}Rb BEC	2×10^{12}	1×10^{-7}

Table 1.2: Differences between bosons and fermions

Bosons	Fermions
integer spin	half-integer spin
Symmetric wave-function	anti-symmetric wave-function
occupation number, $n_i = \frac{N_{states}}{e^{\epsilon_i/k_B T}-1}$	occupation number, $n_i = \frac{N_{states}}{e^{\epsilon_i/k_B T}+1}$
Exhibit Bose enhancement	Exhibit Pauli blockade
Examples: photons, gluons, ^{87}Rb,^{23}Na,^{7}Li	Examples: electrons, protons,^{40}K,^{6}Li

to an interesting observation in quantum mechanics.
Let us define the permutation operation such that:

$$P\Psi(r_1, r_2) = \Psi(r_2, r_1) \tag{1.4}$$

here, Ψ is an eigenket of the Hamiltonian. There are two key observations about this operator, P.
1. $P^2 = 1$, which means by applying the operator twice we recover the original state.
2. Since the Hamiltonian is invariant under permutation, we can find a simultaneous set of eigenkets to describe the system.
After some linear algebraic manipulation (refer to section 8.2 in ref. [44]), we realize that Ψ and $P\Psi$ must describe the same state, and since $P^2 = 1$, they can only differ by a normalization factor $= \pm 1$. Hence,

$$\Psi(r_1, r_2) = \pm \Psi(r_2, r_1) \tag{1.5}$$

This means that the wave-functions must be symmetric or anti-symmetric under exchange. Particles with the symmetric property are said to obey Bose statistics, and hence are called bosons. Particles with the anti-symmetric property obey Fermi-Dirac statistics, and hence are called fermions. Some of their striking differences have been summarized in the following table. An atom is said to be a boson if the sum of its spins is a whole integer, and fermion if it is a half-integer. As the phase space density is increased and quantum mechanical behavior is revealed, we observe that bosonic atoms tend to group together and occupy the low-lying states of the system, eventually forming a Bose-Einstein Condensate which is described as macroscopic occupation of the ground state of the system- BEC) as ρ goes over 2.612 [22, 44]). The phase space density, $\rho = n\lambda^3$, is the dimensionless quantity that signifies the number of particles in a box of volume equal to the cube of the de Broglie wavelength.

The phenomenon of Bose-Einstein condensation is quite unique. It is perhaps the only thermodynamic phase transition that is driven purely by particle statistics and has nothing to do with their interactions. At a phase transition, all thermodynamical variables undergo an abrupt change. This characterizes a critical temperature, T_c. Analogous to a liquid-gas phase transition, the particles can co-exist in two states at the critical temperature. However, below the critical temperature, the gaseous vapour condenses to liquid droplets. Similarly, below the critical temperature, the gaseous bosons condense into a BEC. But unlike normal particles, its not their separation in space, but in momentum space that defines this transition. The condensed particles of a BEC all occupy a single quantum state of zero momentum, while normal particles have a distribution of finite momenta [7].

For fermionic atoms, things are different. The Pauli exclusion principle prohibits them from occupying the same state, so as the temperature decreases, they start occupying the low-lying levels of the system. Since only one particle can occupy a state, not all can be in the ground state and they start occupying the next-available energy state. Thus, in the quantum-degenerate regime, all states below some energy (called the Fermi energy) are filled, giving us a fermi sea. It is this filling of lower energy levels that gives rise to fermi pressure. As a gas of atoms increases its phase space density and enters the quantum degenerate regime, we notice that its momentum distribution spreads even more than what would be expected for a classical Maxwell distribution. This differentiates fermions from classical particles or bosons (since bosons have a much narrower momentum distribution eventually leading to a BEC). In fact it this fermi pressure that is responsible not just for identifying ultra-cold fermionic atomic gases [1], but also for the gravitational stability of massive compact celestial objects like white dwarfs and neutron stars [71].

In this thesis, we shall concern ourselves with three atomic species: ^{87}Rb and ^{85}Rb - which are bosons, and ^6Li, which is a fermion.

1.3 Motivation

Before delving into the details of this thesis, it is important to discuss briefly the motivation for realizing quantum degenerate gases in a system of ultra-cold atoms. Due to its low densities, the interaction between constituent atoms is minimal. In fact, it has been shown that this interaction can be tuned from being highly repulsive to attractive by way of Feshbach resonances (for example [63]). Excellent control over the laser and magnetic fields involved gives us the ability to perform very precise measurements on such quantum systems. This precision and tunability makes these experimentally realized quantum systems prime candidates for being **quantum simulators**.

As Feynman pointed out [37], the ability to store and process superpositions of numbers gives immense parallel computing powers to a quantum computer. A highly controllable quantum system made of a quantum degenerate gas (QDG) of ultra-cold atoms can be used to simulate other more complicated quantum systems, for example electrons in a material. While QDGs might not be the best candidate for factoring large numbers, they are strong contenders to realizing several interesting condensed

Table 1.3: Increase in phase-space density during various stages of a BEC experiment

Stage	Temperature	Phase space density
Atomic source	$300^0 C$	10^{-17}
Slowing	30mK	10^{-12}
Cooling	1mK	10^{-9}
Trapping	1mK	10^{-6}
Evaporation	100nK	> 1

matter hamiltonians, for example, the Bose-Hubbard Hamiltonian [58]. The ample interesting physics that remains to be explored is driving several research programs in the area.

1.4   The experimental route

As a result of Liouville's theorem [80], the application of conservative forces cannot change the volume that the ensemble occupies in phase space. Hence, in order to change the phase space density, we have to apply a non-conservative force on the atoms. Such a force is applied by lasers while laser cooling and trapping, and can change the phase space density by over eight orders of magnitude to about 10^{-6}. The details of how this works theoretically and experimentally constitute the bulk of this thesis and are explained in later chapters. The basic idea is that lasers enable laser cooling provide a force that is proportional to the atomic velocity and its direction is opposite to the atomic motion, hence providing a damping mechanism which slows the atom down, ultimately cooling the ensemble. The final six orders of magnitude are spanned by evaporative/sympathetic cooling [50], where the atoms are loaded into optical or magnetic traps and the hotter ones are allowed to escape by lowering the trap depth. As the remaining atoms thermalize, the ensemble gets colder, and eventually reaches the quantum degenerate regime.

The following table shows order-of-magnitude values for different stages of a typical experiment that produces quantum degenerate gases [80].

Ever since the production of the first BEC in 1995[33], and fermi degenerate gas in 1999[26] the basic structure of the route to degeneracy has not changed by much. Techniques with laser cooling, for example polarization gradient cooling or Raman cooling schemes [48],[21] have enabled experiments to reach a higher phase space density before the evaporative cooling phase of the experiment. Minimizing losses in the evaporative cooling phase requires starting with a colder, denser sample. Proposals for novel schemes to achieve this are constantly being devised.

1.5   Outline of this thesis

This thesis primarily discusses the first step to degeneracy- production of ultra-cold ensembles of rubidium and lithium. It starts with the theoretical details of laser cooling and trapping in chapter 2. The next chapter (chapter 3) contains all the

details of the experimental requirement and the laser setup that was built in our lab to enable us to cool two bosonic species, ^{85}Rb and ^{87}Rb and fermionic ^{6}Li. Chapter 4 deals with summarizing the details of a atomic source for lithium-6. Chapter 5 describes the vacuum system and the control system for the experiment, and recently added preliminary data from our first ensembles of ultra-cold lithium and rubidium. Chapter 6 deals with the planning and progress of the first experiments that we aim to achieve with these ultra-cold atoms- namely looking for feshbach resonances and studying the effect of DC electric fields on them.

Finally some more technical and theoretical details such as spectral broadening mechanisms and details of the laser setup are explained in the Appendix.

Let us, then, be up and doing,
With a heart for any fate ;
Still achieving, still pursuing,
Learn to labor and to wait.

A Psalm of Life : Henry Wadsworth Longfellow

Chapter 2

Laser cooling and trapping - A theoretical perspective

There's a certain slant of light,
On winter afternoons,
That oppresses, like the weight
Of cathedral tunes.
Heavenly hurt it gives us;
We can find no scar,
But internal difference
Where the meanings are.

There's a certain slant of light: Emily Dickinson

This chapter presents a theoretical picture of the mechanisms underlying laser cooling and trapping. The interaction of photons with atoms can be classified into two types: the coherent interaction (corresponding to stimulated scattering), and the incoherent interaction (corresponding to spontaneous scattering events). The coherent interaction generates the dipole potential that is used for optical trapping of atoms and is described in section 1. The (near-resonance) incoherent interaction leads to laser cooling and trapping and will be described in subsequent sections. The interaction of a simple two-level atom with near-resonant light, and the force it experiences due to scattering photons will be considered in section 2.

Atoms experience a laser light below the atomic resonance frequency experience a dissipative force retarding its motion, similar to a viscous force, which is explained in section 3. By extending the same geometry to three dimensions, we can slow down an ensemble of atoms in all three directions of motion. However, the slow atoms are not trapped. In order to trap the atoms, magnetic fields are introduced to create a magneto-optical trap, as explained in section 4. It was discovered that several different mechanisms were responsible for cooling of the atoms below the expected temperature limits, and they are discussed in section 5. To conclude this chapter, we will branch off from a single atom picture and look at the effect of laser cooling on the ensemble at large, discussing temperature and entropy changes in the last section.

2.1 The Dipole Force

2.1.1 Classical Oscillator Model

An atom in a light field $\overrightarrow{E}$ has an induced dipole moment that oscillates with frequency ω. This dipole moment is given by:

$$\overrightarrow{d} = \alpha \overrightarrow{E} \tag{2.1}$$

where α is the polarizability given by [65]:

$$\alpha = 6\pi\epsilon_0 c^3 \frac{\Gamma/\omega_0^2}{\omega_0^2 - \omega^2 - i(\omega^2/\omega_0^2)^3\Gamma} \tag{2.2}$$

Here, ω_0 is the frequency of the transition (classically, the natural frequency of the oscillator), and Γ is the line-width of the transition. The interaction potential of the induced dipole moment with the driving field $\overrightarrow{E}$ is simply

$$U_{dip} = -\frac{1}{2}\overrightarrow{d}.\overrightarrow{E} = -\frac{1}{2}\epsilon_0 c Re(\alpha)I \tag{2.3}$$

The **Dipole Force** is the conservative force that results from the gradient of this interaction potential.

$$F_{dip} = -\nabla U_{dip} = \frac{1}{2\epsilon_0 c}\text{Re}(\alpha)\nabla I(r) \tag{2.4}$$

The scattering rate corresponding to absorption and spontaneous re-emission of photons is given by:

$$\Gamma_{sc}(r) = \frac{1}{\hbar\epsilon_0 c}Im(\alpha)I(r) \tag{2.5}$$

Substituting the expression for polarizability and implementing the rotating wave approximation (which is valid for large de-tunings $|\delta| = |\omega - \omega_0| << \omega_0$), gives the following expressions for the energy and scattering rate:

$$U_{dip}(r) = \frac{3\pi c^2}{2\omega_0^3}\frac{\Gamma}{\delta}I(r) \tag{2.6}$$

$$\Gamma_{sc}(r) = \frac{3\pi c^2}{2\hbar\omega_0^3}(\frac{\Gamma}{\delta})^2 I(r) \tag{2.7}$$

2.1.2   A more quantum view

The effect of electric fields on atomic levels can be treated as a second order perturbation (Stark effect) with the interaction Hamiltonian given by:

$$H = -\overrightarrow{d}.\overrightarrow{E} \tag{2.8}$$

and the energy levels given by [70]

$$\delta E_i = \Sigma_{j\neq i}\frac{|<j|H|i>|^2}{E_i - E_j} \tag{2.9}$$

Note that the change in energy of an atomic level depends on the coupling between the different states- or what is generally known as a dipole matrix element. To describe the system quantum mechanically, we apply the dressed state picture [59] in which both the atom ($\Delta E = \hbar\omega_0$)and the photons ($E = \hbar\omega$) are quantized. For a two-level
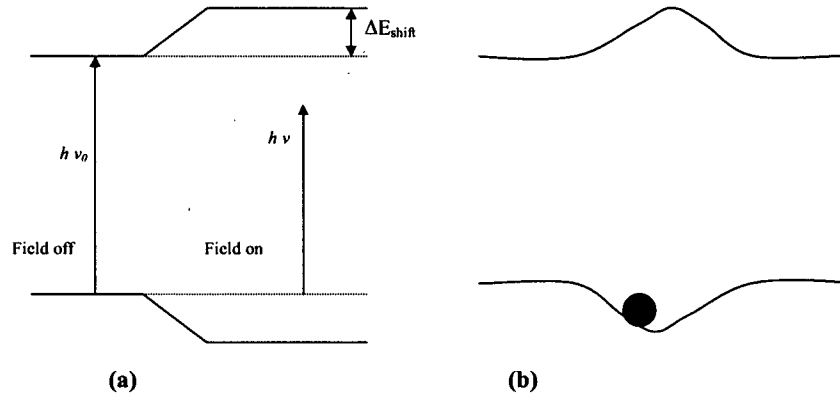
Figure 2.1: Schematic diagram showing the effect of an electric field on a two level atom. (a) The energy levels are moved in opposite directions if the field is red de-tuned to the resonance. (b) In case of a spatially in homogeneous field, such a Gaussian laser beam, the shifted energy levels create an energy minima in which atoms can be trapped.

system, diagonalizing the 2 × 2 matrix of the interaction Hamiltonian [59] gives the energy shifts to be:

$$E_{(ground/excited)} = \pm \frac{3\pi c^2}{2\omega_0^3} \frac{\Gamma}{\delta} I \qquad (2.10)$$

This is remarkably similar to the classical treatment of the dipole potential (Equation 2.6). This induced energy shift is commonly known as the **light shift** or **ac stark shift**. It is this ac stark shift in the energy levels that is used to form a trap for atoms. If $\delta < 0$, then the trap is red de-tuned and atoms are attracted to the minima of the trap, and vice versa for a blue de-tuned trap. The interference of laser beams produces a periodic intensity pattern, and hence a periodic energy shift that is used to make an optical lattice.

2.2 The Scattering Force

Photons have momentum, meaning if a beam of photons scatters off of a target, it must exert some force on the target due to the change in momentum of the photons. To better understand the origin of this force, consider a microscopic picture consisting of one atom and a beam of photons. Each time an atom absorbs a resonant photon, it receives a momentum kick of $\hbar k$ in the direction of the incoming photon. The absorbed photon is then spontaneously emitted in a random direction, and after many absorptions, the average of the momentum vectors of the emitted photons goes to zero. Atoms absorbing counter-propagating photons would be slowed down over time. This provides a force that slows down atomic motion. For one-dimensional motion, this scattering force would be given by:

$$F_{scatt} = photon\ momentum \times scattering\ rate \qquad (2.11)$$

The scattering rate is given by $\Gamma\rho$, where Γ is the spontaneous decay rate of the upper level, and the co-efficient ρ is the fraction of the population in the upper level. Solving the optical Bloch equations for a two-level atom in the presence of an oscillating electric field, gives the steady-state population of level 2 (the upper level) to be [64]:

$$\rho = \frac{\Omega^2/4}{\delta_0^2 + \Omega^2/2 + \Gamma^2/4} \tag{2.12}$$

Here, Ω is the Rabi frequency (the oscillation frequency between the ground and excited state in the presence of resonant light). The Rabi frequency and the saturation intensity are related by the following expression:

$$\frac{I}{I_{sat}} = \frac{2\Omega^2}{\Gamma^2} \tag{2.13}$$

Here, $I_{sat} = \pi hc/3\lambda^3\tau$ by definition, with τ being the decay time for the transition. Combining these definitions gives the following expression for the scattering force:

$$F_{scatt} = \frac{\hbar k\Gamma}{2} \frac{I/I_{sat}}{1 + I/I_{sat} + 4\delta_0^2/\Gamma^2} \tag{2.14}$$

We can see that for high intensities, the maximum limiting value of this force is $F_{max} = \hbar k\Gamma/2$, which is supported by the fact that for high intensities the steady state population of the upper level approaches $1/2$. This maximum force is employed in slowing of atoms (see Zeeman slowing mechanism in Chapter 4).

2.3 Optical Molasses

From the previous section we see that an atom received a momentum kick in the direction of the incoming photon. If the atom has some velocity v in the direction of the incoming photon, it would see the light Doppler shifted to a lower frequency, and hence a de-tuning of $\delta = \delta_0 - kv$, where k is the wave-vector, $k = 2\pi/\lambda$. This gives us a force, F_+ (assuming the photon is coming in the +x direction), where:

$$F_+ = \frac{\hbar k\Gamma}{2} \frac{I/I_{sat}}{1 + I/I_{sat} + 4(\delta_0 - kv)^2/\Gamma^2} \tag{2.15}$$

If we add another laser beam in the -x direction (counter-propagating with respect to the previous beam), then the force on the atom due to this second laser beam would be:

$$F_- = -\frac{\hbar k\Gamma}{2} \frac{I/I_{sat}}{1 + I/I_{sat} + 4(\delta_0 + kv)^2/\Gamma^2} \tag{2.16}$$

Intuitively, one would think that if two laser beams with the exact same characteristics are incident on an atom in opposite directions, the forces induced by them on the atom would cancel in each other out. This is true for an atom at rest, but for a moving atom F_+ and F_- do not cancel. In the approximation that the velocity of

the atom is small, such that $|kv| \ll \Gamma$ and $|kv| \ll |\delta_0|$, we obtain the following expression for the total force [34, 38]:

$$F_{molasses} = 4\hbar k^2 \frac{I}{I_0} \frac{v(2\delta\Gamma)}{[1 + (2\delta/\Gamma)^2]^2} \qquad (2.17)$$

Figure 2.2 depicts the process in a schematic diagram. For red de-tuned light ($\delta < 0$),
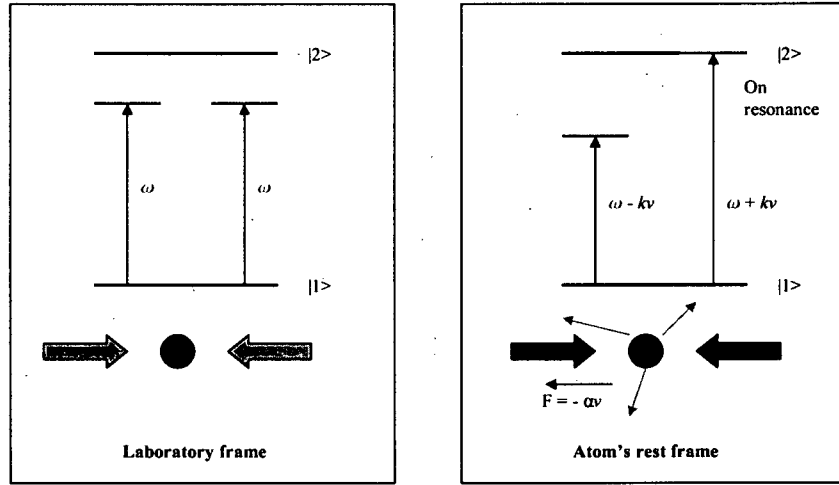
Figure 2.2: Schematic diagram showing the effect of counter propagating beams below resonance frequency on an atom. [Left] 2 beams are not absorbed by an atom at rest. [Right] If the atom is moving in a particular direction, it sees the laser in the opposing direction doppler shifted to the resonance frequency, and gets a momentum kick in the opposite direction to its motion.

the force described in Equation 2.17 would be opposite to the direction of propagation of the atom, and can be thought of as a damping force

$$F_{molasses} = -\alpha v \qquad (2.18)$$

Here alpha is the damping co-efficient whose value can be determined from equation 2.17. We can see, therefore that light exerts a damping, frictional force on the atom. An analogy of this damping force is the viscous drag force experienced by a particle in a viscous fluid, and hence the name "optical molasses". It is important to note that this simple treatment to explain optical molasses only works for $I \ll I_{sat}$. A more detailed description of the different mechanisms that contribute to the actual phenomenon is explained in reference [34].

The simple one-dimensional picture of an atom in the presence of counter-propagating laser beams can easily be extended to three-dimensions. This eventually leads to slow, cold atoms at the intersection of the six counter-propagating laser beams. While the atoms get slowed down and accumulate at the center of the orthogonal intersecting

beams, they do not remain trapped in the region. Since the spontaneous emission of the photons is in random directions, the atomic velocities become randomized and the atoms execute a random walk, and eventually can diffuse out of the region of intersection of the laser beams.

It is quite appealing to think that a trap for neutral atoms can be created that is based solely on absorption and spontaneous emission. However, this idea has a fundamental flaw that was pointed out using the Optical Earnshaw theorem [9]. By analogy to the Earnshaw theorem in electrostatics (which states that it is impossible to trap a charged particle with static electric fields), it can be shown that it is impossible to trap a small dielectric particle at a point of stable equilibrium in free space by using only the scattering force of radiation pressure. If the scattering force is proportional to the photon intensity (as is the case for optical molasses), it will have zero divergence, and would correspond to an unstable trap [4]. However, if some external field alters this proportionality in a position dependent way, a stable trap can be formed. By maximizing the gradient of this scattering force, the trap could be made deeper.

2.4 Magneto-Optical Trap (MOT)

By a clever choice of laser polarization and presence of magnetic fields, the molasses region can easily be converted to a trap for cold-atoms. The most widely used trap for ultra-cold neutral atoms employs such a combination of optical and magnetic fields, and hence is called a magneto-optical trap (MOT). Originally proposed by J. Dalibard, the first such trap was successfully demonstrated in 1987 [29]. This simple and robust technique employs external fields in order to change the scattering force in a position dependent way (as discussed in the previous section) resulting in MOTs being the most successful example of atom traps.

To understand the trapping mechanism of a MOT, let us begin by considering a two-level atom constrained to move along in one dimension with two counter-propagating laser fields. Furthermore, consider the two levels of the atom to contain magnetic sub-levels. This time the two levels of the atom contain magnetic sub-levels. Let the ground state be a $J = 0$ state (only one $m_J = 0$), and the excited state be a $J = 1$ state (three possible magnetic sub-levels, $m_J = 0, \pm 1$). In the presence of a magnetic field, the excited state levels split into three different energy levels due to the Zeeman effect, with the energy depending on the strength of the magnetic field. This is illustrated in Figure 2.3.

Such an inhomogeneous magnetic field is produced by two parallel current carrying coils with current flowing in opposite directions. This configuration generates a quadrupole magnetic field. The field is zero at the center of the coils and increases approximately linearly for small displacements around zero. To provide cooling, the counter-propagating laser beams are de-tuned below resonance. The beams propagating in the $\pm z$ direction have $\sigma^{\pm}$ polarization and thus drive the $m_J = \pm 1$ transitions respectively. An atom in the $+z$-direction is resonant with the σ^- beam that drives the $m_J = -1$ transition. Now that the atom preferentially absorbs one of the laser beams, it undergoes momentum kicks in the direction opposite to its motion, and
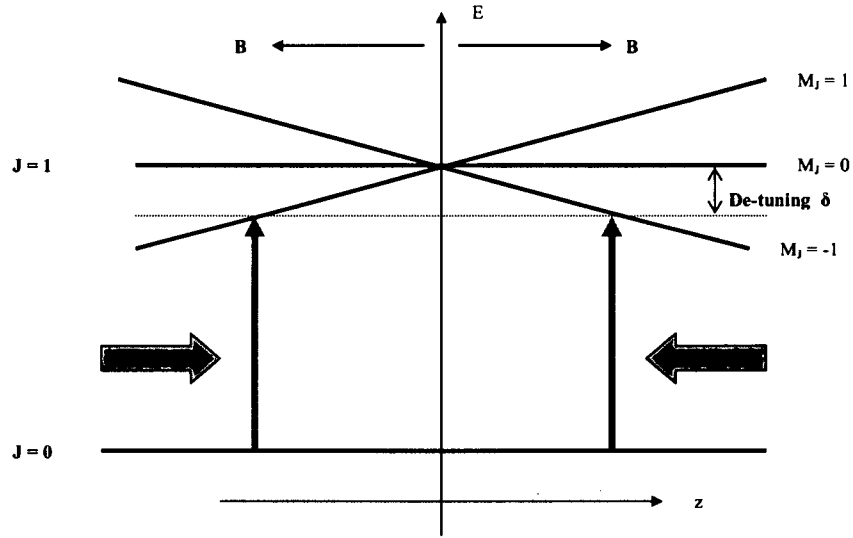
Figure 2.3: Schematic showing the energy levels of a two level atom in the presence of a magnetic field with J=1 being the upper state.

hence is pushed towards the center of the cooling region. Due to the symmetry of the setup, the beams in all six directions (along with cooling the atoms) provide a force on the atom that is directed towards the center of the cooling region. This means that in addition to the frictional force discussed in the previous section, the atom also experiences a position dependent restoring force, $F = -\kappa z$. The spring constant κ is determined to be [4]:

$$\kappa = \frac{\alpha g_e \mu_B \nabla B}{\hbar k} \tag{2.19}$$

Here, α is determined by Equation 2.18, g_e is the g-factor for the atom and μ_B is the Bohr magneton.

MOTs have come a long way since J. Dalibard's proposal and Bell Labs demonstration of the first MOT with sodium atoms in 1987 [29]. This robust trap is used for studies of quantum optics, chaos and precision measurement, along with being the first step towards quantum degeneracy (as it increases the phase space density by about 12 orders of magnitude). The one-dimensional picture and the explanation described above is an over-simplified one. In subsequent sections we shall consider the different cooling mechanisms inside a MOT, and also the loss mechanisms that determine the atom number and the temperature of an ensemble of trapped ultra-cold atoms.

2.5 Cooling Mechanisms and their limitations

In the simplified picture of laser cooling, we have not considered what determines the final temperature of the ensemble. Different cooling and heating mechanisms that occur inside the trap and their limitations set the final temperature of the atom

cloud. In this section, we shall discuss some of the relevant mechanisms that cause both heating and cooling- how they work, and the cooling limits imposed by them.

2.5.1   Doppler cooling

The details of the Doppler cooling process are explained in detail in references [22, 38, 59]. Looking at the microscopic picture, the force from a single laser beam (along the z-direction) on an atom can be described as:

$$F = F_{abs} + \delta F_{abs} + F_{spont} + \delta F_{spont} \tag{2.20}$$

Here, F_{abs}, the force due to absorption is the same as the scattering force discussed in Section 1. The force due to spontaneous emission, F_{spont} averages to zero, since the photons are emitted in random directions. In order to find the sources of heating in the ensemble, consider the fluctuations, δF_{abs} and δF_{spont}. Each absorption (or emission) changes the atomic velocity by v_r, the recoil velocity, where $v_r = \frac{\hbar k}{m}$, and k is the wave-vector of the photon absorbed. Since the scattering process is completely random, it causes the photon's velocity to execute a random walk, with each step size being v_r. We can assume that the velocity distribution follows Poisson statistics. This randomness causes the mean-square velocity in the time interval t, to increase as:

$$\overline{v^2}_{abs} = v_r^2 R_{scatt} t \tag{2.21}$$

due to absorption, and

$$\overline{v^2}_{spont} = \eta v_r^2 R_{scatt} t \tag{2.22}$$

due to spontaneous emission. Here, R_{scatt} is the scattering rate. The factor $\eta = <cos^2\theta>$ is the average over the angular spread of velocities, $v_{r-z} = \hbar k cos\theta/m$. Adding up the forces due to contribution of all these affects, and employing Newton's second law gives:

$$\frac{d}{dt}(\frac{1}{2}m\overline{v^2}) = \frac{d}{dt}\frac{1}{2}m[\overline{v^2}_{abs} + \overline{v^2}_{spont} + \overline{v^2}_{scatt}] \tag{2.23}$$

Substituting, the values of the mean-square velocities from the two previous equations leads to

$$\frac{d}{dt}(\frac{1}{2}m\overline{v^2}) = [\frac{1}{2}mv_r^2 R_{scatt} + \frac{1}{2}m\eta v_r^2 R_{scatt} + \frac{1}{2}m2\overline{v}_{scatt}\frac{d}{dt}\overline{v}] \tag{2.24}$$

Now, if we add the other counter-propagating beam, the scattering rate doubles, and we have one-dimensional molasses. In that case, we already know the force due to scattering from Equation 2.18, and the equation reduces to:

$$\frac{d}{dt}(\frac{1}{2}m\overline{v^2}) = [\frac{1}{2}mv_r^2(1+\eta)2R_{scatt} + \overline{v}F_{molasses}] \tag{2.25}$$

Extending the case to all three dimensions would give us the value of $\eta = 1$. Substituting in $\eta = 1$, and the value for the molasses force, we arrive at:

$$\frac{d}{dt}(\frac{1}{2}m\overline{v^2}) = [\frac{1}{2}mv_r^2 4R_{scatt} - \alpha\overline{v^2}] \tag{2.26}$$

For the equilibrium condition, the sum of all the forces must be zero. Using this fact in the equation, and solving for $\overline{v^2}$ gives:

$$\overline{v^2} = \frac{1}{2}mv_r^2\frac{4R_{scatt}}{\alpha} \tag{2.27}$$

Substituting the values of the friction co-efficient, α, and the scattering rate, R_{scatt} that we computed earlier in 2.18 and 2.7 respectively, we can get an expression for $\overline{v^2}$ in terms of frequencies. To relate this to temperature, we could use the equipartition theorem that equates kinetic energy to temperature by the relation $\frac{1}{2}m\overline{v^2} = \frac{1}{2}k_BT$. After making these substitutions, we finally arrive at an expression for temperature of the form:

$$k_BT = \frac{\hbar\Gamma}{4}\frac{1 + (2\delta/\Gamma)^2}{-2\delta/\Gamma} \tag{2.28}$$

The minima of this function occurs at a red de-tuning of half the natural line-width, or $\delta = -\Gamma/2$, and defines a minimum temperature of

$$T_D = \frac{\hbar\Gamma}{2k_B} \tag{2.29}$$

This is the **Doppler Cooling limit**. It gives the lowest temperature that can be achieved in an optical molasses for a simple two-level atom. Since this heating is due to spontaneous emission, which is an integral part of the laser cooling process, it cannot be avoided. The Doppler limit for cold rubidium is $144\mu K$, and for lithium is around $140\mu K$ [80]. However, experimental measurements of temperature of a cloud in optical molasses gave results that were much different and colder than this temperature. An analysis of the mechanisms that were responsible for this is addressed in the subsequent subsections.

2.5.2   Polarization Gradient cooling

This cooling scheme relies on different couplings of a multi-level atom with light. Let us start with an atom in the ground state with $J_{ground} = 1/2$ and $J_{excited} = 3/2$ and these levels be further split into magnetic sub-levels (as shown in Figure 2.4).

When counter-propagating laser beams of orthogonal polarizations shine on the atom, they interfere to form a spatially inhomogeneous pattern as shown in Figure 2.4 for $\sigma^+ - \sigma^-$ light and two orthogonal linear polarizations. As discussed in Section 1, atoms in a light field are subjected to an ac stark shift that depends on the coupling between the different states. The m_F sub-levels are coupled differently to the excited state depending on the polarization of light- thus creating a spatially inhomogeneous potential for (orthogonally) linearly polarized light, but a constant potential for circularly polarized light.

In case of linearly polarized beams, an atom with sufficient kinetic energy climbs the potential hill only to be optically pumped to the bottom of the hill for another m_F state. This process occurs continually until the atom has lost enough kinetic energy that it is not even be able to climb the potential energy curves of the m_F states. This cooling process is called **Sisyphus cooling** [23].
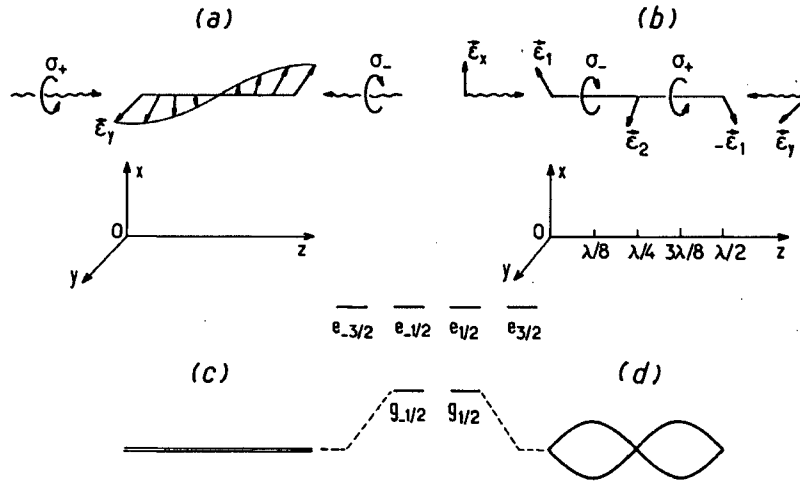
Figure 2.4: Schematic diagram showing the energy levels of a multi-level atom, with J=1 being the lower state, in the presence of counter-propagating laser beams. Because the resultant polarization is differs as a function of distance (as demonstrated in (a) for $\sigma^+ - \sigma^-$ configuration and in (b) for 2 orthogonal linear polarizations), the energy levels are shifted appropriately (as demonstrated in (c) and (d)) leading to novel cooling mechanisms [figure from [23]].

However for the case of a MOT, with orthogonal circularly polarized light, the energy levels simply shift by the same amount for all the m_F states, and no Sisyphus cooling takes place. A more subtle mechanism is responsible for sub-doppler cooling in this case. When the atom starts to move, the symmetry of the atom-photon interaction is broken. An atom moving towards a σ^+ beam sees it to be closer to resonance and gets optically pumped (eventually) to the highest m_F state. The scattering rates are altered due to this re-distribution of the population as the atom moves. This leads to a much stronger scattering force (compared to the one that causes doppler cooling)[23].

An estimate of the equilibrium sub-doppler temperature is characterized by the ac stark shift induced by the light, and an approximate expression (assuming $\delta \gg \Gamma$) is given by [4]:

$$k_B T = \frac{\hbar \Gamma^2}{4|\delta|} \frac{I}{I_{sat}} \tag{2.30}$$

This analysis of sub-doppler cooling breaks down when the atomic momentum approaches the momentum from a single photon kick- when the de Broglie wavelength is comparable to the laser wavelength and a full quantum treatment of the problem is required.

2.5.3 Recoil limit

As mentioned earlier, the recoil velocity corresponds to the momentum kick that the atom gets in a single spontaneous emission process. Since this process is of stochastic nature, it would lead to a heating affect. The temperature scale corresponding to this kinetic energy is called the **recoil temperature limit**

$$k_B T_r = \frac{(\hbar k)^2}{2M} \tag{2.31}$$

The recoil limit temperature for cold rubidium is 370 nK, and for lithium is aproximately 6μK [80]. The final temperature of a MOT was proposed to be around a few times this recoil temperature mostly because of two convincing arguments [53]. First, as mentioned before, the last photon for the cooling process would leave the atom with at least one $\hbar k$ momentum, and since this momentum is in a random direction, it would contribute to heating. Second, the polarization gradient cooling mechanism requires the atom to be localized within approximately $\lambda/2\pi$ in order to be subjected to only a single polarization in the spatially varying electric field. The uncertainty principle requires the atom to have a momentum uncertainty of around $\hbar k$. Thus the recoil limit sets the lower limit for temperature in the presence of light, and to get colder than that, the laser fields have to be switched off.

2.6 The macroscopic picture

The discussion so far in this chapter about temperature has been only for a single atom. Intuitively, this contradicts the very definition of temperature, which is actually a statistical property of the entire ensemble. Nevertheless, it is convenient (and now the norm) to describe the kinetic energy of an atom in terms of (absolute) temperature units by the simple conversion in one dimension:

$$\frac{1}{2}mv^2 = \frac{1}{2}k_B T \tag{2.32}$$

The other very important reason why the idea of temperature adopted in laser cooling in scientifically inappropriate is due to the fact that the system (atoms + photons), although in its steady state, cannot be called in thermal equilibrium [59]. It is interesting to think of temperature in terms of the entropy of the system. The well-collimated beam of photons interacts with the matter and gets spontaneously emitted in a random direction. Since there are numerous choices for the frequency, polarization and direction of the out-going photon, the change in entropy of the photon due to absorption and spontaneous emission is enormous. When compared to the entropy change in the atomic ensemble, we are led to realize how inefficient this cooling scheme is. In other words, laser cooling makes a very inefficient refrigerator for atoms [18]. Laser cooling is a demonstration of how light is able to create order in matter. In fact it is a more interesting observation of the fact that the bulk entropy of matter is lower than the thermal equilibrium for matter (in a stationary state). Of course, the second law of thermodynamics ensures that the photon entropy is

increased.

A particularly interesting calculation of entropy change and the efficiency of different kinetic effects of resonant light on matter are considered in reference [75]. Here, matter entropy is given the standard Boltzmann treatment (the sum of entropies of the excited and non-excited particles), and the photon entropy is calculated using Bose statistics. Using Hänsch and Schowlow's original proposal [42] for laser cooling, and assuming a temperature change by a factor of 2500 using laser cooling, the ratio of entropy change in the atomic beam and the entropy change in the photon beam was calculated to be 10^{-5}.

In spite of being an inefficient process, laser cooling is remarkable with respect to dramatically narrowing the phase space density of the atomic ensemble, owing to the fact that lasers can be used both for velocity spread narrowing and spatial confinement. It is important to note here that the velocity distribution must be narrowed to enable cooling, and it is this narrowing (and hence change in phase space density) that distinguishes cooling from a velocity-selection process.

None may teach it anything,
'Tis the seal, despair,-
An imperial affliction
Sent us of the air.
When it comes, the landscape listens,
Shadows hold their breath;
When it goes, 't is like the distance
On the look of death..

There's a certain slant of light: Emily Dickinson

Chapter 3

Getting the light- The laser system for experiment

It little profits that an idle king,
By this still hearth,among these barren crags,
Match'd with an aged wife, I mete and dole
Unequal laws unto a savage race,
That hoard, and sleep, and feed, and know not me.

Ulysses: Alfred Tennyson

In the last chapter, we discussed the theory of what enables laser cooling. For an experimental demonstration of it, the emphasis is on different things. The stability, accuracy and tunability of the laser system are some of the experimental challenges that will be addressed in this chapter. It gives an overview of the theoretical considerations during design of the laser system that just stems out of the atomic level structure in section 1. The rest of the chapter is about how to implement the desired laser system.

In section 2, we give a brief introduction to semi-conductor diode lasers that are the workhorse for the experiment. In section 3, we describe why and how diode lasers are modified to form a tunable external cavity laser. Section 4 deals with how to make the lasers accurate (using saturated absorption spectroscopy) and stable (using frequency modulation locking technique). Section 5 discusses how the light is amplified at the desired frequency (using slave lasers and acousto-optical modulators). The last section (section 6) gives all the technical details, including the optical setup and various settings for the entire optical setup that enables laser cooling and trapping of all three species ^{6}Li, ^{87}Rb and ^{85}Rb.

3.1 Requirements for the laser system

From the theoretical study of laser cooling, the following salient points are reiterated.
Multi-level atomic structure
Even simple alkali atoms that have only one electron in their outer shell, have a much more complicated level structure than those discussed in the previous chapter. This leads to an increase in the number of energy levels the excited electron could decay to. If an atom undergoing cooling due to repeated absorption and spontaneous re-emission decays to another energy level which is not on resonance with the lasers, it gets lost from the ensemble being cooled. This leads to the use of more lasers to have a 'closed' cooling transition, ensuring that the atoms don't get lost from laser cooling transition.

Frequency of the laser cooling light

As discussed in the previous chapter, the laser light must be red de-tuned by a few natural line-widths to the resonance frequency of the cooling transition. Since laser frequency is of the range 10^{14} Hz and the line-width 10^6 Hz, it requires the laser frequency to be very accurate and also stable for the duration of the experiment. Not just that, the ability to tune laser frequency closer or farther from resonance during the experiment is also required to enable efficient cooling.

With that in mind, let us start with a look at the atomic energy levels of the atoms of interest.

3.1.1 Lithium

We start with ^{6}Li. With only three electrons, it is the alkali atom that seems closest to hydrogen with respect to electronic structure. Due to its light mass, the splitting in energy levels due to the fine and hyperfine interaction are small compared to all other alkali atoms. The existence of two hyperfine ground states makes it necessary to have two frequencies present in the light to laser cool lithium. One is for the transition that actually enables cooling due to fast absorption and spontaneous emission cycles (F=3/2 to the $2P_{3/2}$ manifold)- hence called cycling or cooling transition laser. The other laser frequency (tuned to F=1/2 to the $2P_{3/2}$ manifold) pumps the atoms that decay into the other hyperfine transition back to the cycling transition, and hence called re-pumper. Figure 3.1 shows the energy level diagram of lithium with the relevant transitions that are used for laser cooling.

Since the ground state hyperfine splitting is only 228 MHz- the re-pump light can easily be attained by frequency shifting some light using acousto-optical modulators instead of having a different frequency stabilized laser system. However, because the cooling transition light, which is near the F=3/2 to F'=5/2 transition, can very easily off resonantly excite a transition from F=3/2 to F'=3/2 (only 2 MHz away) and this state can decay to the lower ground state, the atom is very quickly pumped out of the upper ground state. This de-pumping happens much more quickly than in Rubidium where the hyperfine splitting in the excited state is much larger than the atomic line-width and implies that much more re-pump light is required to keep the atoms trapped in the case of Lithium. In addition, because the number of re-pump photons scattered is on the same order as the number of cooling transition photons, the re-pump light should ideally also have the correct polarization to also contribute to trapping in the MOT. It also makes sub-doppler cooling inefficient, since the multiple transitions spoil the polarization gradient.

Another important thing to note is the hyperfine splitting of the excited state, $2\,P_{3/2}$, is just 4.4 MHz- which is even smaller than the natural line-width of the transition (6 MHz). This means that all spectral features due to this hyperfine splitting would be washed out and we can think of it as a single energy level. This enables us to approximate lithium atom as a three-level system with two ground, and one excited state, instead of a much more complicated multi-level atomic structure.
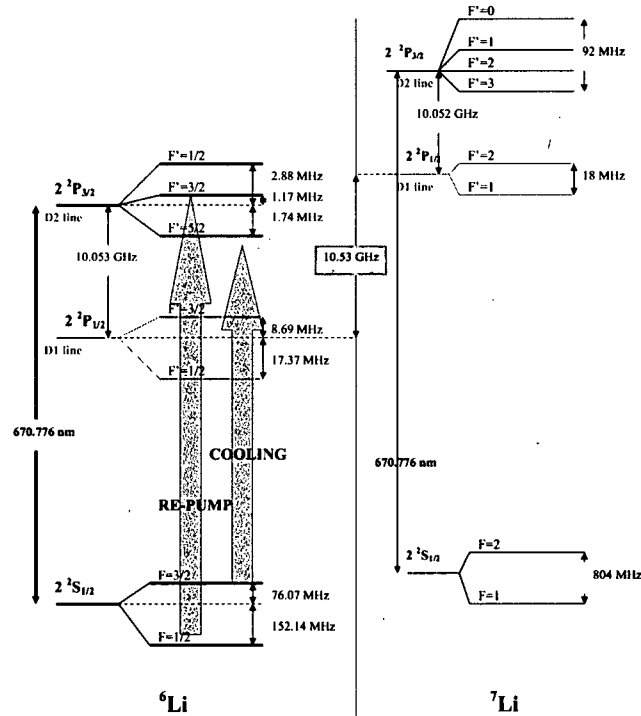
Figure 3.1: Schematic of lithium energy level diagram with the laser cooling and re-pump light shown for ^{6}Li. ^{7}Li energy levels are shown for comparison- and also since they overlap with some ^{6}Li transitions. Refer to [47] for more accurate frequencies.

3.1.2 Rubidium

Unlike lithium, the hyperfine splitting in rubidium are much bigger, as shown is Figure 3.2. It cannot to approximated as having a single excited state. First, the ground state hyperfine splitting for rubidium isotopes is in the GHz range, which is too large to be spanned by an acousto-optical modulator. So, different lasers are required for cooling and re-pump transitions. Second, the excited state hyperfine splitting is wide enough for the corresponding spectral features to be far apart. The advantage is that since the corresponding de-pump transition (F=2 to F'=2 and F=3 to F'=3 for 87 and 85Rb respectively) is many line-widths away from the cycling transition, the probability of an atom decaying out of the cycling transition is much lower and the re-pumper beam does not have to be strong. In fact, a weak beam in just one direction works well enough.

3.2 Semiconductor lasers

All the laser light needed for the experiment is generated by semi-conductor diode lasers. This section provides a brief introduction to them. For a more complete discussion, please refer to [84] or [76]. The principle of operation of semi-conductor
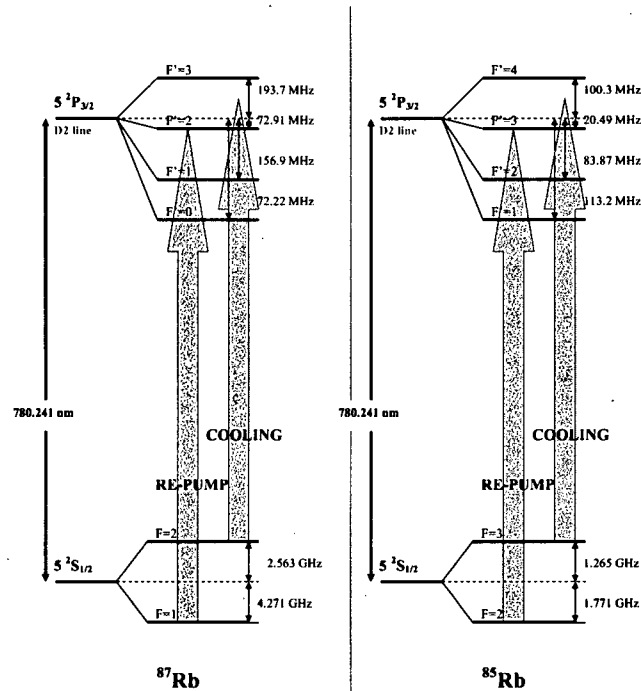
Figure 3.2: Schematic of rubidium energy level diagram with the laser cooling and re-pump light shown for both [87]Rb and [85]Rb. Refer to [28] for more accurate frequencies.

lasers is similar to light-emitting diodes (LEDs) in the sense that light is produced by radiative recombination of electrons and holes at a p-n junction. If we forward bias a heavily doped p-n junction diode, this radiation can stimulate the radiative re-combination process, hence realizing laser action (if amplification exceeds the loss-rate) [64].

Figure 3.3 gives a schematic diagram of a simple semi-conductor diode. The lasing action is initiated by the injection current [20]. Due to the structure of laser cavity, the output beam is diverging and astigmatic. This is corrected by using collimation lenses and a cylindrical lens pair (or anamorphic prism pair) respectively. Figure 3.4 is a graph of injection current vs. optical output from one of the laser diodes being used in the lab. It clearly shows the onset of lasing action at a threshold current around 30 mA.

Diode lasers usually do not employ mirrors for feedback. This is because the refractive index at the semiconductor-air interface is large enough to give considerable reflection. In fact, higher power (over 50mW) diodes are usually coated with a high reflectance material at the back surface and reduced reflectance coating on the output facet [20]. However, since the diode itself makes the laser cavity, the laser is highly susceptible to temperature changes.

The laser emission wavelength is determined by the band-gap of the semi-conductor material. Hence, we use two different types of lasing materials to give us light for
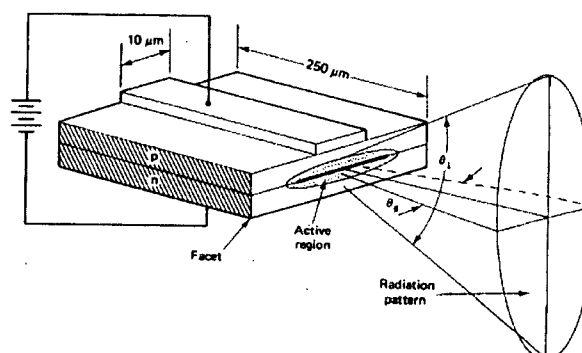
Figure 3.3: Schematic of a simple p-n junction laser. from [76]. The ellipsoidal mode inside the p-n junction results in the diverging, astigmatic radiation pattern we see.

Table 3.1: Table of all the diode lasers being used in the lab and their characteristics.

Property	Rb Masters	Rb Slaves	Li Master	Li Slaves
Laser	GH0781JA2c	MLD780100S5P	RLT6720MG	HL6535MG
Manufacturer	SHARP	Intelite	Roithner	Opnext
Polarity	cathode gnd.	cathode gnd.	anode gnd.	cathode gnd.
Th. current	29 mA	30 mA	30 mA	55 mA
Op. current	73-84 mA	80-100 mA	67 mA	163-168 mA
Op. temperature	18 ^0C	18 ^0C	30 ^0C	78 ^0C
Spec. wavelength	784 nm	780 nm	670 nm	658 nm
Op. wavelength	780 nm	780 nm	671 nm	671 nm
Spec. out. power	50 mW	100 mW	10 mW	90 mW
Actual out. power	50 mW	70 mW	6 mW	35 mW

rubidium (780nm) and lithium (671nm). Details of these lasers is given Table 3.1.

For spectrometry purposes we require tunability of the laser wavelength and stability. This is accomplished by making an external cavity that can be fine-tuned to the right frequency, or modulated as required.

3.3 External Cavity Diode Lasers- the Master laser system

The master laser system is the primary laser system that is the source of the ultra-stable, well-collimated light required for laser cooling. The following subsections describe the different components that constitute the external cavity of the master laser system, and how they provide the required tunability. For a more detailed study of External Cavity Diode Lasers, a recent book about them [85] is highly
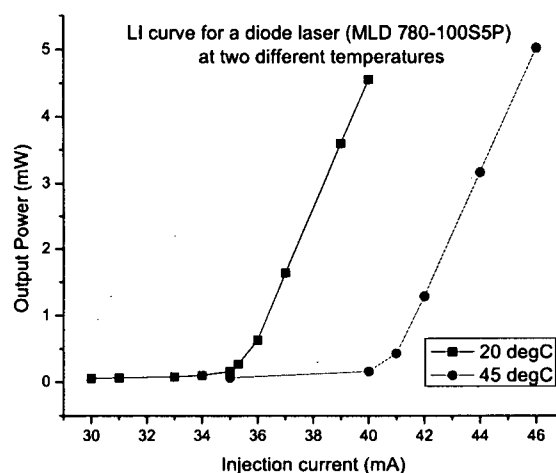
Figure 3.4: Graph showing the output power of the laser beam versus injection current for a Rb master laser for two different temperatures. We can clearly see the transition from LED to Laser mode, and how this threshold behavior is affected by the temperature of the lasing cavity.

recommended.

3.3.1 Theory

To build an external cavity, it is important to have an anti-reflection coating on at least one of the facets of the diode laser, so that its operation is purely conducted by the cavity we build. However, due to the technical expertise required [32], we decided to not AR coat our lasers and see their performance first. Apart from the occasional mode-hops, our master lasers work just fine.

An external cavity diode laser (ECDL) uses frequency selective feedback to provide the user with narrow bandwidth and tunability, something that is desired by several atomic physics experimentalists. This wavelength selective feedback is provided by an inexpensive frequency selective optical element, for example, a grating or etalon. Two popular optical configurations exist that employ diffraction gratings: Littrow [8] and Littman- Metcalf [43]. We chose the simpler Littrow configuration for our master lasers.

In the Littrow arrangement, first-order diffraction from the grating is coupled back into the laser diode and the directly reflected light forms the output beam. The back facet of the diode laser chip (which has a high reflective coating) forms the other reflective surface for the cavity. In the Littrow configuration, the output frequency is controlled by the angle of the grating and therefore the center frequency of the optical feedback provided by the diffraction from the grating. The disadvantage of the Littrow configuration over the Littman-Metcalf configuration is that the output

beam angle is coupled to the output frequency since it is also determined by the grating angle. The addition of a turning mirror parallel to the grating transforms this angular shift into a simple translation of the beam which helps to circumvent this problem [13]. Figure 3.5 shows a schematic of this modified Littrow configuration, and a picture of the inside of our master laser- which is based on this modified Littrow configuration.

Apart from the optical setup, there are temperature and current controllers for the diode laser system, and a simple protection circuit inside the box. The masters are further acoustically isolated by a rectangular enclosure lined with one inch thick sheets of lead-lined foam lead-lined foam (Soundcoat- product number EL510HP1) to further reduce vibrations.
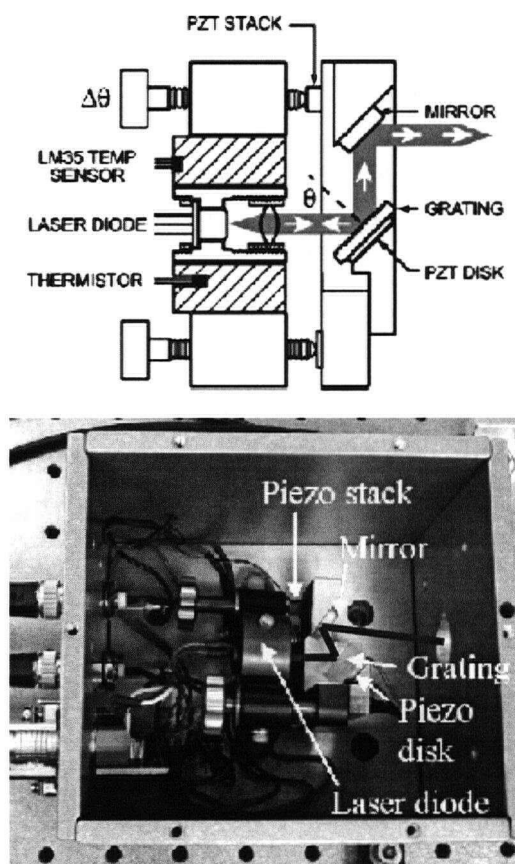
Figure 3.5: Top: Schematic of the master laser setup using littrow configuration ECDL from [13]. Bottom: Picture of a master laser for Rb trapping

3.3.2 Nuts and Bolts: putting together a master laser

The technical details of putting together a master laser have already been described in great detail in an earlier lab report [2]. Here I would outline the things that we discovered about our lasers that were implemented later in the design.

First, the importance of getting rid of low frequency acoustic resonances should be emphasized. The reason is that a couple of master lasers for rubidium showed strong acoustic resonances at frequencies of less than 1kHz, the range of normal speaking frequencies. This made it very hard to lock the laser while people were talking. Even otherwise, it would pick up a lot of acoustic noise. We got rid of it by stretching the springs in the mirror mount(which increases the spring constant, pushing resonance frequencies higher), and inserting small pieces of sorbathane in it to dampen them. The effect of this is demonstrated in Figure 3.6, which shows the acoustic resonances before and after this modification.

The method used to determine the acoustic resonances was simple. A program was written in LabVIEW to automate a function generator and acquire data from an oscillosope. A sinusoidal signal was sent frequencies to a speaker kept next to the master. A zoomed in view of an absorption spectra (on the side, so as to see maximum effect of amplitude change). Due to the speaker, there was some sinusoidal feature that appeared on the absorption spectra. The plot shown is a linear graph of this peak-to-peak voltage of that noise feature as a function of frequency. an enhancement of that Vpp indicates an acoustic resonance. In principle, a change in the phase of the sinusoidal signal would have indicated a resonance better. However, it as hard to obtain, since the laser kept fluctuating a bit in frequency during the course of one such measurement.
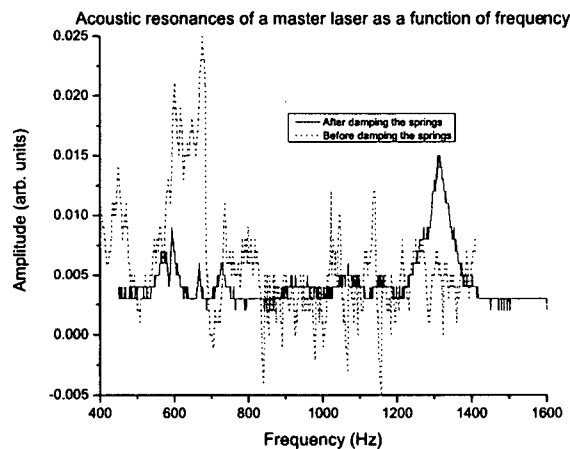
Figure 3.6: Graph showing the effect of stretching and damping the mirror mount springs. The acoustic resonances become less prominent and also shift to higher frequencies.

Another observation was rather stumbled upon by accident. When forced to adapt a grating mount machined for a lithium system for a rubidium laser, we noticed that instead of getting multiple positions through optical alignment where the threshold current lowered by a few mA, and one moderately good one; there was a single broad region of very good injection, where the threshold current lowered by a few mA. This laser also scanned all four absorption lines for rubidium beautifully, while some others showed a lot of mode hops. After careful observations, it was noticed that the angle of the reflected light (used as feedback for injection) was not well aligned with the output of the laser in the previous configuration. The diffraction grating was tilted horizontally in one direction using additional washers on the grating mount. This led to the the incoming feedback light being aligned with the laser diode output, and hence a more stable feedback cavity.

3.4 Locking the laser

The laser system requires not only tunability over a relatively longer range (few tens of GHz) to identify spectral features, but also control of a frequency within a few MHz precision while laser cooling atoms. This is accomplished by a frequency modulation locking scheme described below.

A semi-conductor diode laser has a gain profile that spans several nanometers. By making an ECDL, the wavelength can be tuned (but not mode-hop free) over a range of about 5 nm by the rotation of the grating alone, and over a wider range with suitable temperature adjustment. The PZT transducer allows electronic adjustment of the cavity length, enabling tunability of over 20 GHz by ramping the voltage on it. However, for laser cooling experiments we want to be spanning a few natural line-widths (MHz range) close to the transition. So, first, the laser frequency must be more sharply defined, both absolutely, and in terms of the laser band-width. The former is achieved via saturated absorption spectroscopy that gives us an absolute frequency reference to compare our lasers to. By deriving an error signal from our spectrum, and locking to it, we can narrow the band-width of our lasers to within 5 MHz. These methods will be discussed in this section.

3.4.1 Saturated Absorption Spectroscopy

As is pointed out in the appendix A, Doppler broadening is the dominant contribution to the width of atomic spectral lines. It occurs because atoms are moving around randomly in the measurement vapour cell, and have a distribution of velocities, and hence they see the frequency of the light beam doppler-shifted by an amount depending on the velocity. This leads to an inhomogeneous broadening of the spectrum (because each atom interacts differently with the light [refer to Appendix A for details]). There are several ways to get around the problem- some of them being crossing the laser beam with respect to the atomic beam, doing two-photon transitions and saturated absorption spectroscopy. The last of these methods is the most preferred method for laser cooling experiments- mostly due to its simplicity.

In this subsection we shall discuss how saturation absorption spectroscopy works

starting with the basic idea in a simple two-level atom picture, and moving on to explaining the spectra obtained in the lab. Parts of the explanation are based on chapter 8 of [38], and can be consulted for a much more detailed explanation.

Two-level atom: the simple picture

Let us start with a two-level atom for simplicity. Let N_1 be the number-density of atoms in the lower level, and N_2 in the higher energy level. The atoms have a broad temperature-dependent Maxwell-Boltzmann distribution of velocities. We define

$$\int_{-\infty}^{\infty} N_1(v)dv = N_1 \tag{3.1}$$

And similarly,

$$\int_{-\infty}^{\infty} N_2(v)dv = N_2 \tag{3.2}$$

The total number density, $N = N_1 + N_2$ always remains conserved. In a simple saturated absorption setup, a strong pump beam and a relatively weak probe beam are passed through the atomic vapour cell in counter-propagating direction. The pump (being stronger) interacts with atoms with velocity $v = \frac{\omega - \omega_0}{k}$, where ω is the frequency of the laser, ω_0 is the atomic resonance frequency, and k is the wave vector ($k = 2\pi/\lambda$). It ends up putting the atoms it addresses due to their Doppler shift into the upper state, hence N_2 increases, thus burning a "hole" in the population of the ground state. Refer to Figure 3.7 for a schematic diagram explaining this effect. As mentioned above, this hole is burnt at a certain velocity, the doppler shift of which corresponds to the resonance frequency of the transition. The width of the hole is given by the familiar equation from any laser textbook describing such phenomenon.

$$\Delta\omega_{hole} = \Gamma(1 + \frac{I}{I_{sat}})^{1/2} \tag{3.3}$$

When the pump and probe lasers are far away from the atomic resonance, they address atoms of velocities in opposite directions. However, at the atomic resonance, they both address the $v = 0$ atoms. The atoms preferentially absorb the pump beam, since it is stronger. This leads to a reduction in probe absorption, which is measured on a photodiode. We can clearly observe the "saturation effect" caused by the presence of the pump beam in probe's absorption profile.

Extension to multi-level alkali atoms

This simple picture can easily be extended to a more realistic, multi-level atomic system like that of the alkali atoms that we use. These would have several saturated absorption peaks- each corresponding to transition from one of the hyperfine ground states to an excited hyperfine ground state that is allowed by the transition rules.
In addition to these saturated absorption peaks, we also observe additional features referred to as cross-over resonances. To explain this effect, we will consider a three-level system- with two ground, and one excited state, as shown below. (In fact, owing
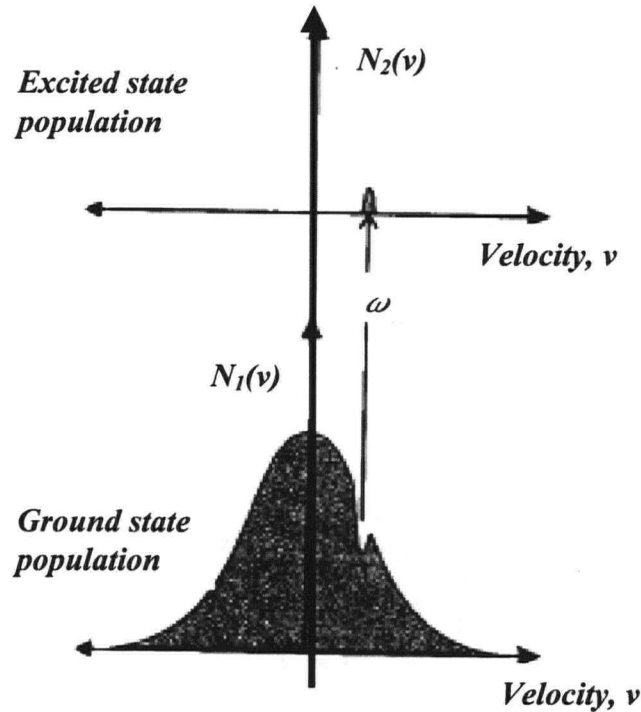
Figure 3.7: Schematic diagram illustrating the hole burning mechanism in saturated absorption spectroscopy. A hole is burnt in the ground state population for a certain velocity class due to the pump beam that leads to a decrease in the probe absorption. Figure from [38].

to the splitting in lithium's energy levels, it can be approximated as such a three level system).

When the incident light is between the two resonances, an atom moving at a certain velocity v, such that kv is equal to half of the energy difference between the resonance energies, $h\nu_1$ and $h\nu_2$, sees the light doppler shifted to an atomic resonance. This is illustrated in the figure 3.8. If the atom is moving towards the incoming photons, it would see the frequency blue-shifted to the more energetic resonance frequency- in our case ν_1, and if it is moving away from the photons, it would see it red-shifted by the same amount- which would correspond to the second resonance frequency ν_2. This leads to the presence of an additional saturated absorption peak exactly in between the two resonances. Since most atoms have a quite a few resonances, we observe not only plenty of saturated absorption peaks corresponding to a particular transition, but also additional cross-over peaks that occur exactly between the two resonance frequencies.
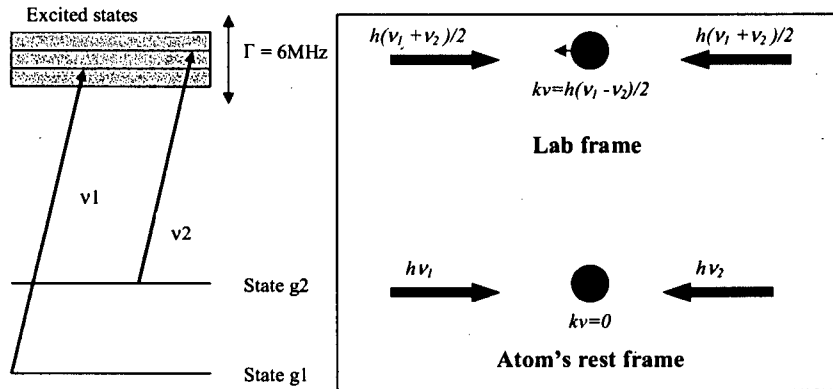
Figure 3.8: Schematic of a three level atoms, with two ground and one excited state. The figure also shows how the moving atom sees light at two resonances from one that is at a wavelength between the two resonances in the lab frame. This doppler shifted light leads to cross-over resonances.

3.4.2 Frequency modulation locking scheme

A technique like saturated absorption spectroscopy provides us with an absolute measure of the frequency of the laser by comparing it with the resonance in the atoms. After we have this frequency, we need to ensure that the laser stays "locked" to this frequency by some sort of an electronic feedback loop. This is accomplished by a frequency modulation locking scheme that I shall describe below. For detailed theoretical description please refer to reference[11].

To use this technique we modulate the light frequency ν by a small amount $\delta\nu$ such that the light frequency is now given by $\nu = \nu_0 + \delta\nu sin\omega t$. This modulation is achieved by sending the pump through an acousto-optical modulator that shifts and modulates the frequency by a few MHz. Consequently, the absorption signal (or more precisely, the saturated absorption signal)will also be modulated and can be expanded around ν_0 to get:

$$I(\nu) = I(\nu_0) + \frac{dI}{d\nu}|_{\nu_0}(\delta\nu\sin\omega t) + \frac{d^2I}{d\nu^2}|_{\nu_0}(\delta\nu\sin\omega t)^2 + O(\delta\nu)^3 \qquad (3.4)$$

This signal is sent to a home-built circuit, the lock-box, that has a phase-sensitive amplifier, and proportional and integral feedback stages. Here the signal is first multiplied by the sine wave of the same frequency and then time-averaged in order to improve signal-to-noise. The phase between the photo-diode signal and the reference sine wave (ϕ) can be adjusted to give the maximal output signal. So, the output of the amplifier becomes:

$$Output\ Amplitude = \frac{1}{T}\int_0^T I(\nu).\sin(\omega t + \phi) \propto \frac{dI}{d\nu}|_{\nu_0}\delta\nu \qquad (3.5)$$

Hence, we achieve a signal that is proportional to the derivative of the absorption signal. This provides us with the error signal for our feedback controller. As the
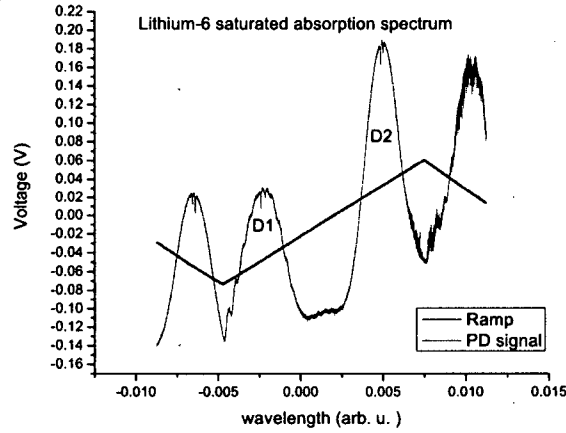
Figure 3.9: Graph showing the absorption spectrum of lithium-6 with the saturated absorption peaks.

Table 3.2: Table of the different transitions at which the master lasers are locked and the frequency shift of the pump beam due to the AOM.

Master laser	Pump freq. offset	Lock transition
Rb-85 cooling	2 × +120MHz	F'=3-F'=4 x-over
Rb-87 cooling	+94 MHz	F'=2-F'=3 x-over
Lithium	+102 MHz	F=3/2-excited states
Rb-87 re-pump	2 × +101MHz	F'=1-F'=2 x-over
Rb-85 re-pump	2 × +103MHz	F'=1-F'=2 x-over

laser drifts in frequency (due to fluctuations in injection current or slow drift of room temperature), the absorption peak also drifts to one side of the previous maxima or another. In order to correct for it, we need a signal that is different on the two sides of the signal. The Lorentzian absorption profile is symmetric on both sides of the resonance, but its derivative is not. It changes signs around the resonance- giving us our locking signal. By using a standard proportional-integral stage feedback loop, with this error signal as the input, we can frequency stabilize our laser to a few MHz. There are two outputs from the lock-box: a slow correction, that changes the PZT voltage, hence changing the length of the laser cavity in order to correct for slow temperature drifts, and a fast correction, that changes the injection current in order to achieve a fast feedback to small fluctuations.
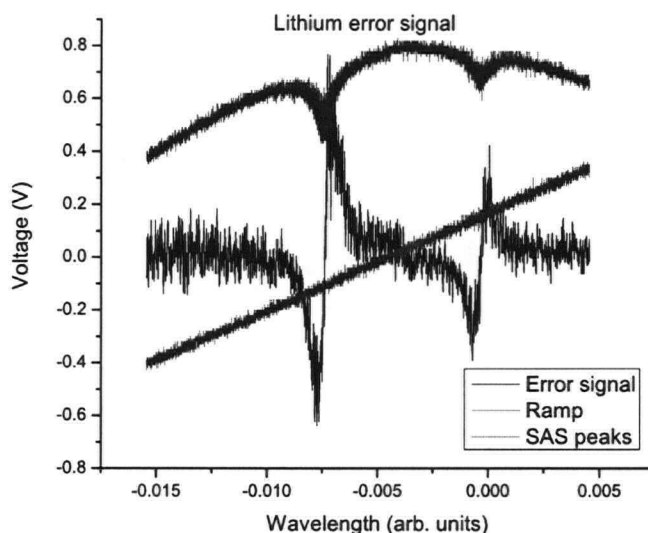
Figure 3.10: Zoomed in view of the absorption spectrum for lithium-6 showing the saturated absorption peaks. Also shown on the graph is the error signal obtained by the lock box for that signal.

3.5 Amplification at the right frequency

While the Master lasers are frequency-stabilized, they do not have enough optical power to do the experiment. Also, due to the acousto-optical modulator in the locking scheme, the laser are locked to a frequency offset from the resonance. Besides, we also need tunability in our frequency shift from resonance of our trapping light. All this is accomplished by a series of optical components that are described in the following subsections.

3.5.1 Injection locking- the Master-Slave relationship

As pointed out before, the masters don't generate enough power to do the experiment. So, we use additional diode lasers acting as amplifiers to generate more light at the desired frequencies. This amplification stage consists of high power lasers typically running (longitudinally) multi-mode around the desired frequency. They are frequency stabilized using the method of optical injection locking. For more information on this scheme, please refer to [41]. Basically, some of the frequency-stabilized master light is sent back into the slave, which drives the multi-mode laser to lase at that particular mode (hence the master-slave name scheme). If the injected light is in the gain profile of the slave laser, which can be tuned by the current and temperature of the slave diode lasers, and is spatially mode-matched, it will enhance that particular spectrally narrow mode. So, the power coming out of the laser does not

Table 3.3: Table showing all the AOMs being used for the experiment.

AOM name	Location	Purpose	Frequency
Rb-85 lock SP*	Master table	Freq. mod. lock	+120 MHz
Rb-87 lock SP	Master table	Freq. mod. lock	+94 MHz
Lithium lock SP	Master table	Freq. mod. lock	+102 MHz
Rb-87 re-pump lock SP*	Master table	Freq. mod. lock	+101 MHz
Rb85 re-pump lock SP*	Master table	Freq. mod. lock	+103 MHz
Lithium DP1	Master table	Tune around resonance	-100 MHz
Lithium DP2	Master table	Shift to re-pump	+114 MHz
Rb-87 re-pump DP	Feshbach table	Tune around resonance	+80 MHz
Rb-87 pump SP	Feshbach table	Tune around resonance	-86 MHz
Rb-87 trap DP	Feshbach table	Tune around resonance	+80 MHz
Rb-85 re-pump DP	Feshbach table	Tune around resonance	+80 MHz
Rb-85 pump SP	Feshbach table	Tune around resonance	+59 MHz
Rb-85 trap DP	Feshbach table	Tune around resonance	+80 MHz

* = pick second order

increase (contrary to a naive presumed and completely wrong understanding), it is just that the power at that particular frequency that increases sharply. The principle of this feedback mechanism is the same as that of the grating stabilized feedback lasers being used as masters. The only difference being that in this case the optical feedback is provided by another laser and not from the reflection from the grating.

3.5.2   Acousto-optical modulators

Acousto-optical modulators are used in atom trapping experiments for several purposes: as frequency shifters, modulators or fast shutters. We use them for frequency modulation (for locking the master lasers) of light, and also for shifting.

The principle of operation is simply based on a crystal whose index of refraction changes sharply with density. When a high-power acoustic wave is sent to the crystal, it travels through it as a longitudinal sound wave creating regions of high and low density. This turns the crystal effectively into a diffraction grating. This is the effect which leads to the diffraction pattern that we observe when we send light through the crystal. The key difference being that since the diffraction grating itself is moving at sound velocity, the diffraction orders are also frequency shifted. The zeroth order is unaffected by the frequency of the acoustic wave, while the different orders of diffraction are frequency shifted, and their angular separation (understandably) varies as the frequency of the input acoustic wave.

The following table lists all the AOMs used for laser cooling purposes and some of their characteristics. Further details are described in Appendix B.

3.5.3 Fiber network for diagnostics

In order to ensure that all the slave lasers are injected and running at the right frequency (i.e. still injected and injected at the right frequency), some light from each slave is coupled into a diagnostics fiber. These are 1550 nm telecom fibers that were donated to UBC from JDS Uniphase. All these fibers goto a N-input: 1-output fiber switcher box. The output light from the switcher comes to the diagnostic setup. For each rubidium and lithium light, a Fabry-Perot interferometer and a vapour cell (in case of lithium, light is sent through the heat pipe being used to get the lock signal) constitute the diagnostics set-up. Light out of the fiber is split into these two components. They give us information about the frequency characteristics of the laser. Besides, we can always sweep the master laser, and watch the slave follow (or not follow, as is mostly the case). This diagnostic setup has provided us with an effective tool for trouble-shooting by enabling us to identify which laser is not working properly.

3.6 More technical details

Through the previous sections, we presented a step-by-step picture of the optical setup for experiments. Since my project primarily included the feshbach resonances experiment, most of the experimental details are relevant for that experiment. However, the same locked masters (after being amplified) also feed light to two (one in case of lithium) more experiments- the miniature atom trap and photo-association. Details of the objectives of these experiments would be explained in chapter 6. In this section, all the optical components discussed before are combined to describe the big picture- the optical setup for laser cooling and trapping. First, specific details for the rubidium and lithium are presented separately and then we explain the combined setup to make a triple species MOT. Further details are presented in Appendix B.

3.6.1 Details of the rubidium setup

A flowchart like diagram explaining the light flow for a typical rubidium setup is shown in Figure 3.11. On the master table, every laser (cooling and re-pump lights for both isotopes) is locked using appropriate saturated absorption signals, and then amplified so that enough light goes through the fiber-optics cables to the three experiments.

A point to note about the master table setup is that wherever double passing though the AOM was required for frequency shifting- that was replaced by picking the second order of the diffracted beam. This was due to the fact that we had a lot of light coming out of the master laser. It wasn't just more than sufficient for spectroscopy and injecting the slave laser- in fact stray back reflections from the slave laser and the double-pass setup were partly responsible for frequency instability of the masters. Since the back reflected powers were considerably large (mostly due to ineffective polarization optics), we realized that even the 35 dB of isolation provided by the optical isolator was not sufficient to attenuate this light to an insignificant power.

Using a single-pass setup not only got rid of some of the frequency noise on the error signal, but also saved quite a bit of optical components. The interference due to back-reflection, and the aligning beam from the slave laser was solved by inserting a neutral density filter in the path of the injection beam. On the Feshbach experiment
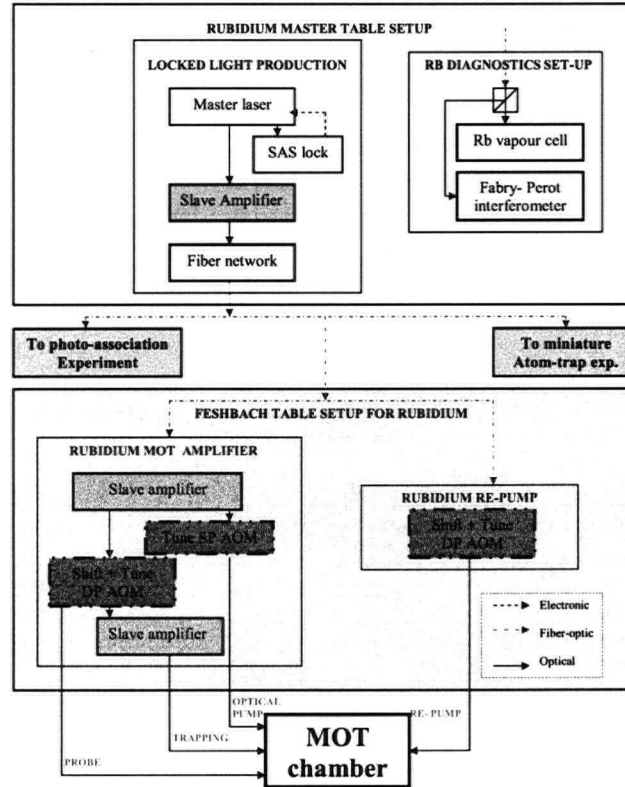
Figure 3.11: Flowchart summarizing the the optical procedure to create light to enable rubidium's laser cooling.

table, while there is enough light after appropriate frequency shifting for re-pump laser beam (recall from section 1 that there is not much light required for rubidium re-pumping), the trapping light has to be amplified in order to have enough power for cooling and trapping and also for detection.

Details of the actual setup including the frequency of various lasers for trapping are explained in the appendix B.

3.6.2 Details of the lithium laser system

Lithium laser system is designed a bit different than that of rubidium, as can be seen in Figure 3.12. This is primarily because of the requirement of a strong re-pump beam that is close to the cycling transition. It employs a single master laser that is locked and then frequency shifted (after being amplified) to inject a slave that gives

cooling light to both experiments. This AOM can be tuned in order to adjust the frequency de-tuning of both trapping and re-pump light- since the output of this AOM forms both the trapping and (after being shifted 228 MHz) re-pump light. Additional tunability is provided by independently tuning the AOM that shifts the laser from cooling to re-pump transition.
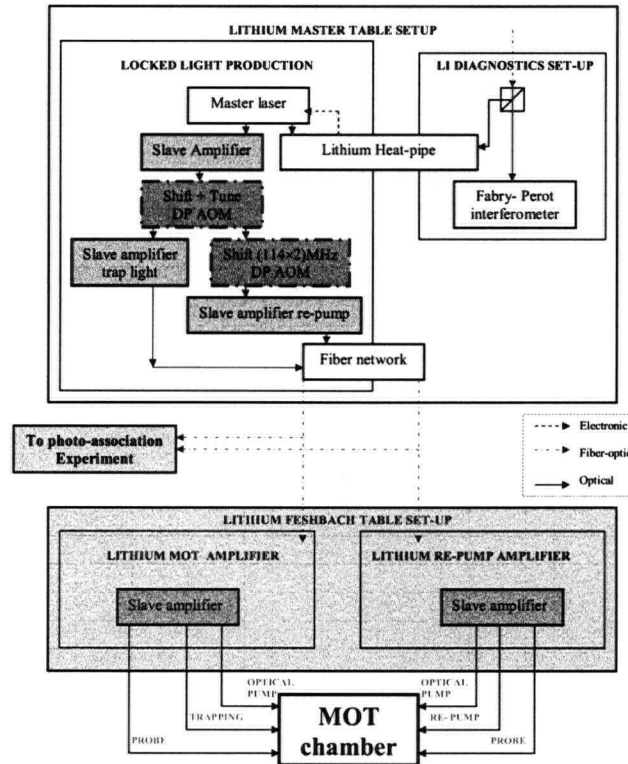
Figure 3.12: Flowchart summarizing the the optical procedure to create light to enable lithium's laser cooling. The diagrams and pictures of the optical setup is shown ahead.

There are no AOMs on the experimental tables for lithium light. So, the Feshbach table setup is pretty simple. The light from the fiber-optic cable is simply amplified to get the required power of the two frequency lights for laser cooling and trapping. An important technical problem was encountered on the master table that could be taken into consideration for future experiments. The distance between the lithium master and slave was around 1.3m. Such a long distance led to alignment problems while injecting the slave, and making it get out of the injection frequently. Since the master table was floating on a foam, with the slave being significantly far away, any small vibrations on the master table led to significant misalignment of the slave beam, and the slave got out of lock very frequently. This problem was temporarily fixed with mode-matching the injection beam with the slave output, and precise alignment. However, it remains a problem. So, it is important to keep in mind that if any of the slaves don't appear to be injected, it would be a wise idea to check the first slave, because it goes out of injection most frequently.

Another important technical detail to keep in mind is that the AOM don't appear to be as efficient for the same focussing for lithium as they are for rubidium. This is because lithium light, having a smaller wavelength, is focussed a lot tighter making the diffraction in efficient. This can be overcome by either using a longer focal length lens or by creating a small divergence by using a 1:1 diverging lens telescope centered around the AOM.

More details of the actual setup, including the actual table setup and the frequency of various lasers are explained in appendix B.

Tho' much is taken, much abides; and though
We are not now that strength which in old days
Moved earth and heaven; that which we are, we are;
One equal temper of heroic hearts,
Made weak by time and fate, but strong in will
To strive, to seek, to find, and not to yield.

Ulysses: Alfred Tennyson

Chapter 4

In Search of an Efficient Atomic Source

Two roads diverged in a yellow wood,
And sorry I could not travel both
And be one traveler, long I stood
And looked down one as far as I could
To where it bent in the undergrowth.

The Road Not Taken : Robert Frost

Here I shall elaborate on the various standard ways of loading atoms into a Magneto-optical trap (MOT) and comment on the efficiency of different procedures. While the calculations and comments in this section are for lithium atoms, similar calculations can be done for any other atom. Due to the significantly different vapour pressure of lithium as a function of temperature, certain techniques prove to be not very efficient (for example loading from background vapour). However, these techniques could be optimal and in fact are widely used in case of other atoms (for example rubidium and cesium are typically loaded from a background vapour).
An optimal design for the atomic source is important since it limits the number of trapped atoms. Since I spent a significant amount of time designing the atomic sources for multiple experiments, I shall briefly describe the loading mechanism for different types of sources and the various considerations to keep in mind while designing the source. At the end of the chapter, I shall conclude by justifying the choices for atomic sources that were made. Hopefully these calculations and the conclusions drawn can provide some guidance during the design of atomic sources for ultra-cold atom experiments.

4.1 Loading a MOT from atomic vapour

Atomic background vapour loading is by far the simplest way to load a MOT. Atoms from a background gas with velocities below the maximum capture velocity of the MOT are trapped in the middle of the intersecting beams. An ensemble of atoms in a dilute vapour has a standard Maxwellian distribution of velocities that is dependent on temperature, and a MOT captures the low-velocity tail end of the distribution. The losses are mostly due to trapped atoms colliding with the more energetic untrapped atoms. Of course, other density dependent losses in a MOT come into effect as well. But we shall just consider this as the loss mechanism to get an order-of-magnitude estimate for the number of atoms that would get trapped in such a configuration.The treatment shown here is based on reference [14], and further details

can be found there or in reference [69]. The calculations I show here have been modified for our experimental setup of lithium atoms. However, they can be extended to any atomic vapour.

The rate at which atoms would be trapped in a MOT is given by some loss rate (γN, where γ is the loss-coefficient, and N is the number of trapped atoms) subtracted from the loading rate (R).

$$\dot{N} = R - \gamma N \qquad (4.1)$$

Solving this differential equation, we get:

$$N(t) = \frac{R}{\gamma}(1 - e^{-\gamma t}) \qquad (4.2)$$

The loading rate is given by [14]:

$$R = \frac{nV^{2/3}v_c^4}{2v_{mp}^3} \qquad (4.3)$$

Here, n is the density of atoms, V is the trapping volume, which is around 4.2 cm^3 for 2cm diameter laser beams. v_c is the maximum capture velocity of the MOT. The stopping force on the atom is provided by the two counter-propagating lasers, and decreases rapidly with velocity. Let us assume that the laser is typically one line-width towards the red away from the resonance frequency. So, the atom would be captured and cooled if the doppler shifted light that it sees is within a line-width from the resonance. Equating the two, we get $v_c \approx \Gamma\lambda$, which for our transition (D2 line for^{6}Li, $\Gamma/2\pi = 5.9$MHz [65]), corresponds to a velocity of around 25 m/s. I shall use this estimate for the capture velocity for the rest of my calculations. The most probable velocity, v_{mp} can be defined as (from any thermodynamics textbook):

$$v_{mp} = \sqrt{\frac{2k_B T}{m}} \qquad (4.4)$$

As mentioned earlier, the loss-mechanism we consider is collisions with background, un-trapped atoms. For simplicity, let us assume that the colliding atoms are at the most probable velocity for simplicity. This gives us the loss coefficient of:

$$\gamma \approx n\sigma v_{mp} \qquad (4.5)$$

The collisional cross-section σ is assumed to be 6.3×10^{-13}cm^2 [69]. This is an underestimate for the loss rate because it assumes the background contains only lithium, but gives us some idea. Combining the above equations, we can determine the steady-state number of trapped atoms, N_{ss}:

$$N_{ss} = \frac{R}{\gamma} = \frac{V^{2/3}}{2\sigma}(\frac{v_c}{v_{mp}})^4 \qquad (4.6)$$

Figure 4.1 shows a graph of the steady state number N_{ss} as a function of temperature. The number of trapped atoms in such a lithium MOT is much smaller than the steady

state number for most other atom MOTs. This has to do with the fact that lithium has a small mass and a very small vapour pressure. However, for some other atoms like cesium, around 3.6×10^{10} atoms have been trapped in a vapour cell loaded MOT [49]. In fact loading from a vapour cell MOT remains the standard method for ultra-cold experiments with Cs, and usually Rb and K as well.

Since the experimental signal is proportional to the number of trapped atoms, it is desirable to have a much bigger number of trapped atoms in the MOT. Also, since any cooling scheme that may be implemented to cool this ensemble further would also lead to losses, we have to start with a much bigger ensemble from the beginning. Hence other techniques must be implemented to increase the number of trapped lithium atoms.
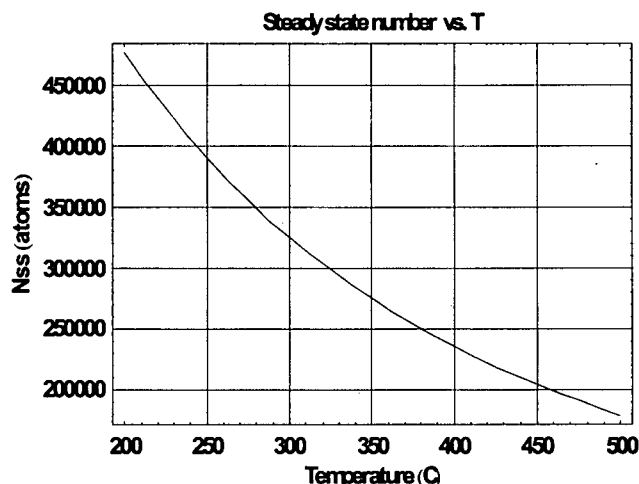
Figure 4.1: The calculated steady state number for trapped atoms in a lithium MOT as a function of temperature.

4.1.1 A note about desorption

It has been experimentally demonstrated that in the presence of intense UV or broad-band light, the number of trapped atoms from certain alkali-metal atomic vapour can be significantly increased [6, 35]. This is due to light-induced atomic desorption (LIAD). When light is incident on the inner surface of the vacuum chamber, the alkali atoms that have coated the inner walls quickly get desorbed and the vapour pressure increases significantly. This leads to a higher number of trapped atoms. Since this light source can be turned on and off fast, the background vacuum can be maintained at low pressures, and the alkali atoms can also be recycled. While this technique has been demonstrated to produce optically thick rubidium, sodium and potassium atomic vapour, the effect of light induced desorption still remains unexplored in lithium and might provide a way for a simple and efficient MOT loading mechanism.

Table 4.1: Difference between the velocity profile of background gas and a beam

Property	Gas	Beam
Distribution	$v^2 exp(\frac{-v^2}{v_{mp}^2})$	$v^3 exp(\frac{-v^2}{v_{mp}^2})$
Most probable v	$\sqrt{\frac{2k_B T}{m}}$	$\sqrt{\frac{3k_B T}{m}}$
Root-mean-square v	$\sqrt{\frac{3k_B T}{m}}$	$\sqrt{\frac{4k_B T}{m}}$
Average velocity $\overline{v}$	$\sqrt{\frac{8k_B T}{\pi m}}$	$\frac{3}{4}\sqrt{\frac{2\pi k_B T}{m}}$

4.2 Loading a MOT from an effusive atomic beam

Let us consider atoms effusing through a small hole of area A_s. The characteristic velocities of such atoms would differ from a Maxwell-Boltzmann distribution of atoms, as outlined in reference[38]. The faster atoms are more likely to pass through the hole and hence the thermal distribution of velocities differs from that of a standard Maxwell-Boltzmann. Table 4.1 shows some key differences (reproduced from [38], pg 152). v_{mp} is the most probable velocity given by equation 4.4 The number of atoms flying out of such a source per second (or the dissipation rate)is simply given by:

$$\frac{dN}{dt} = \frac{n\overline{v}A_s}{4} \tag{4.7}$$

We can calculate the loading rate of such a MOT by simply integrating the distribution of velocities up to the capture velocity of the MOT. Following the calculations shown in Savard's thesis[69], we can get the following expression for the rate at which atoms are effusing from the oven:

$$\frac{dN}{dt} = \frac{2nA_s}{\pi^{1/2}v_{mp}^3} v_r e^{\frac{-v_r^2}{v_{mp}^2}} v_z e^{\frac{-v_z^2}{v_{mp}^2}} dv_z dv_r \tag{4.8}$$

To find the number of atoms for the loading rate calculations, we need to consider appropriate limits on the velocities in radial and axial directions. Let the axial upper limit be the capture velocity of our MOT. To calculate the radial velocity, we find the velocity that the atoms would have so that after traveling a distance d to the MOT with axial velocity being the capture velocity of the MOT, the atom has spread radially only so much that it is still in the trapping region. Thus, the maximum radial velocity is given by:

$$v_{rmax} = \frac{v_c}{d}r_c \tag{4.9}$$

For our experiment, r_c is 1 cm, and d is 15 cm. Integrating over this velocity range, we can get an expression for the loading rate of the MOT.

$$R = \frac{n\overline{v}A_s}{4}(1 - e^{\frac{-v_c^2}{v_{mp}^2}})(1 - e^{\frac{-v_{rmax}^2}{v_{mp}^2}}) \tag{4.10}$$

In order to calculate the steady state number, we need to consider the losses. Let us

Figure 4.2: The calculated loading rate for trapped atoms in a lithium MOT as a function of temperature for an atomic beam source.

consider a maximum velocity, $v_{zmax} = 1000 \times v_c$. We can integrate our distribution up to these maximum velocities to get an approximate value for the total number of lithium atoms coming out in the MOT capture area.

$$\dot{N}_{total} = \frac{n\bar{v}A_s}{4}(1 - e^{\frac{-v_{zmax}^2}{v_{mp}^2}})(1 - e^{\frac{-v_{rmax}^2}{v_{mp}^2}}) \qquad (4.11)$$

This gives the loss rate of:

$$\gamma = \sigma \frac{\dot{N}_{total}}{\pi(d\frac{v_{rmax}}{\sqrt{3/2}v_{mp}})^2} \qquad (4.12)$$

Here, the denominator being an estimation of the area suspended by the solid angle of the collimated beam. The factor $\sqrt{3/2}$ is due to the difference in the velocity profile between a background gas and beam, as discussed earlier.

While we are on a more realistic path, we could include collisions with background vapour of different impurities (not just the hot atoms effusing out of the source), at a pressure of around 10^{-10}torr as a possible loss mechanism. For simplicity with respect to coliisional cross-sections, we assume this background to consist of just lithium. Adding that in our loss rate, we can get a more realistic expression for our losses. By dividing the loading and loss rate, we can get the steady-state number of trapped atoms. Figure 4.3 is a graph of the steady state number of atoms as a function of oven temperature.

4.2.1 Collimation issue

So far we have considered atoms effusing from a hole with no well-defined collimation of the atomic beam. However, we can greatly reduce the angular distribution of our
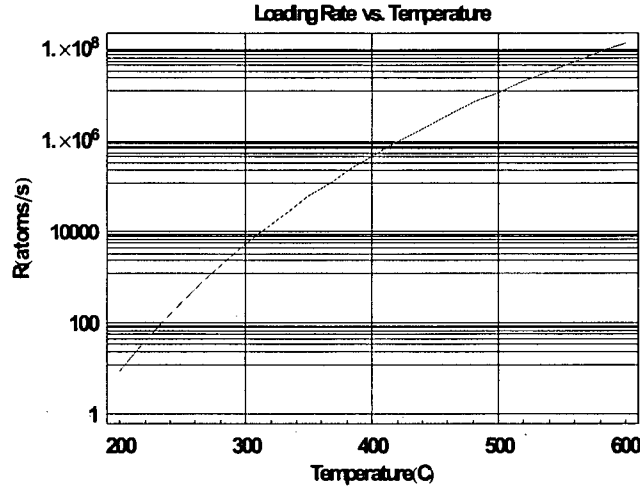
Figure 4.3: The calculated steady state number for trapped atoms in a lithium MOT as a function of temperature for an atomic beam source. We can see an approximately 100-fold increase from a vapour cell MOT.

atomic beam just by making the beam effuse through long channels. The pressure is chosen such that the atoms do not collide with each-other inside the channel. Of course, this decreases the number of atoms coming out of the channel walls. This reduction is implemented in the dissipation rate equation, and the modified equation 4.7 looks like:

$$\frac{dN}{dt} = \xi \frac{n\bar{v}A_s}{4} \tag{4.13}$$

Here, ξ is called the reduction co-efficient. For a cylindrical geometry (which is usually considered), a circular tube with diameter(d) much smaller than the total length(l), the reduction co-efficient is given by [74]:

$$\xi = \frac{4d}{3l} \tag{4.14}$$

Carefully chosen geometries enhance the MOT steady-state number primarily due to three reasons:

1. The flux of atoms is collimated so that more atoms actually arrive at the MOT capture area.

2. The transverse spread of velocities in atoms is decreased, since atoms with high radial velocities do not get out of the channel.

3. Due to the presence of a narrow channel, differential pumping takes place- the experimental chamber is pumped at a much faster rate than the rate at which the source chamber introduces particles. This makes it possible to maintain the experimental chamber at a much lower pressure than in the source (which is orders of magnitude higher due to the partial pressure of hot lithium atoms). A lower background pressure suppresses loss mechanisms due to background collisions thereby increasing the steady state number and the lifetime of trapped atoms.

Figure 4.4 is another graph of the steady state number of atoms for a lithium MOT with the same source, but this time using just a 1/4" thick tube for collimation (hole diameter- 0.03", length- 0.25"). We can see that the steady state number increases for all temperatures. We can thus choose the geometry of the collimator such that the solid angle imposed by the tube covers the MOT area. This increases efficiency of our trapped atoms. Also, longer channels make it easier to maintain the experimental vacuum chamber at a much lower pressure than the source chamber.
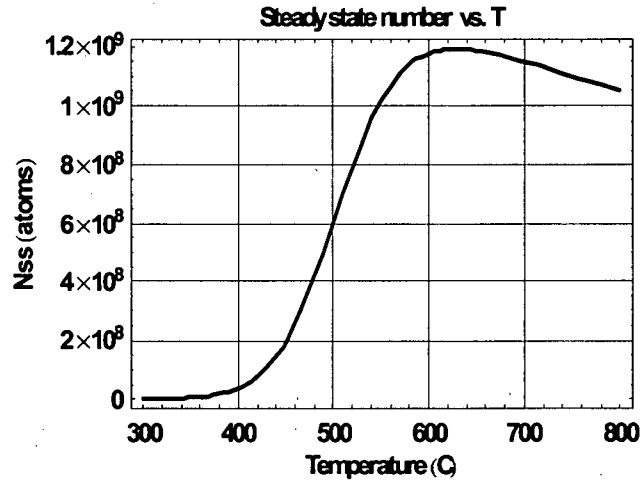

Figure 4.4: The calculated steady state number for trapped atoms in a lithium MOT as a function of temperature for an atomic beam source. We can see an increase in the Nss at all temperatures just by a small collimation of the atomic beam.

4.2.2 Background collisions with Rubidium

In the experiment, we plan to have MOTs of two different species running at the same time. It is therefore important to consider the loading of a lithium MOT in the presence of rubidium vapour. Unlike that of lithium, the vapour pressure of rubidium is high enough to enable loading of rubidium from background vapour at room temperature. The number density of rubidium atoms is given by the ideal gas law:

$$n_{rb} = \frac{P_{vacuum}}{k_B T} \qquad (4.15)$$

where P is th epartial pressure of rubidium at room temperature (around 10^{-8}torr). This gives the loss-rate of:

$$\gamma_{rb} = n_{rb}\sigma\sqrt{\frac{2k_B T}{m_{rb}}} \qquad (4.16)$$

Since the collisional cross-section of lithium-rubidium atoms is unknown, we assume it to be the same as the one we considered for lithium-lithium collisions- 6.3×10^{-13}cm^{-2} (which is probably a good order-of-magnitude estimate). We add

this loss rate to the total loss-rate expression that becomes the sum of three different loss mechanisms, namely loss due to background lithium and rubidium vapour and the loss due to the hot atoms in the lithium atomic beam. This is plotted in Figure 4.5. It is important to note here that rubidium would not be the only contaminant in
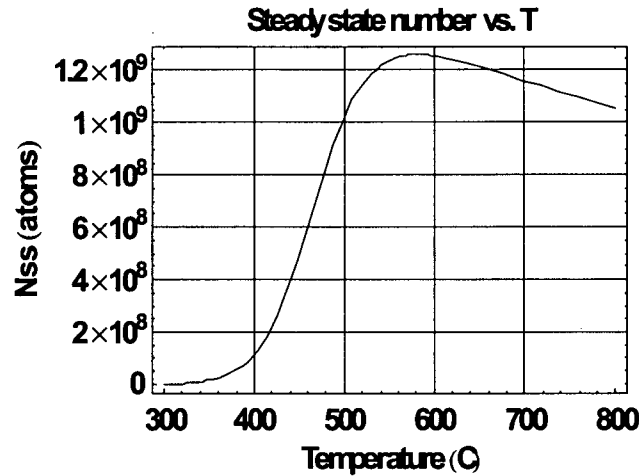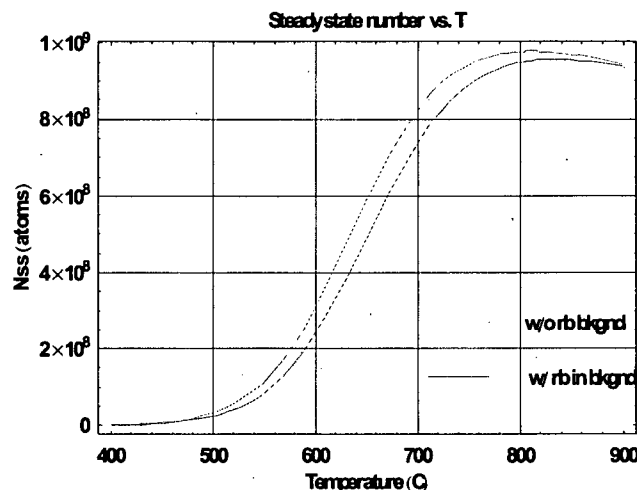

Figure 4.5: The calculated steady state number for trapped atoms in a lithium MOT as a function of temperature for an atomic beam source in the presence of a background of rubidium atoms. We can see a decrease in the Nss due to enhanced collisional losses.

the MOT. There would be background vapour of atmospheric gases and other out-gassing materials that would contribute to the loss-rate. However, this calculation was done in order to provide a rough estimate and hence the other loss-mechanisms (that would be treated in a similar manner) are being ignored here.

4.3 Slowing an atomic beam

The calculations described above give us an over-simplified view of the number of atoms that can be loaded into a magneto-optical trap. There are other loss mechanisms that have not been considered in this picture: for example, fine-structure changing collisions in case of lithium (and rubidium) and three-body collision, light assisted collisional losses and heating losses. Overall, it would not be pessimistic to say that the real steady-state number of atoms would be lower than the estimate that we have calculated (especially because with the experimental chamber vacuum pressure is currently much higher than 10^{-10} torr). Since the the number of atoms is our signal, we need to maximize it. Also, in order to reach degeneracy we need to have additional stages of cooling. At each of these stages, we would be losing atoms. for example, loading into an optical or magnetic trap always leads to loss of some atoms due to heating. Needless to say that there is evaporative cooling as well. In order to increase the number of trapped atoms, we need to have more atoms below

the capture velocity of the MOT. This can be done by starting with a colder atomic beam. Due to partial pressure of lithium as a function of temperature considerations, which is responsible for the atomic oven being run at around 400 ^0C, we cannot have a cold beam of lithium vapour coming out of the atomic source. But additional mechanisms can be used in order to cool the atomic beam in order to make loading more efficient.

One thing to keep in mind is that for ultra-cold experiments, atoms only interact with electric and magnetic fields, because they are suspended in the middle of the vacuum chamber in a magnetic (or optical) bowl. So, any cryogenic technique cannot be implemented. Buffer-gas cooling or stark deceleration has been widely used as universal techniques in chemistry to cool many species. However, these techniques are rather complicated and so far no one has tried them. Moreover, buffer gas cooling usually needs rather high pressures of the cold buffer gas, which would be hard to make compatible with a MOT. There can be simpler ways to cool alkali atoms using magnetic fields or laser light. In this section, I shall summarize some such experimental approaches in this section.

4.3.1 Shifting, chirping or broadening the laser frequency

The loading rate of a MOT is highly sensitive to the capture velocity. As discussed above, the capture velocity depends on the de-tuning of the laser beams from the resonance frequency. So, in order to increase the capture velocity and maximize the number of trapped atoms, the lasers can be further red de-tuned from the atomic resonance. However, this just makes the laser talk to a different velocity class of atoms that are more abundant in the atomic beam. If the red de-tuned laser beam shines opposite to the atomic beam, then it would slow the atoms down by radiation pressure. By carefully choosing the de-tuning frequency, the number of trapped atoms can be enhanced. Such a set-up has been described in reference [19], where the steady state number was increased by five-fold by using a single 115 MHz red de-tuned, circularly polarized slower beam opposite the atomic beam of ^{7}Li atoms. The major drawback of this cooling scheme is that as atoms slow down, they go out of resonance from the laser light. So, if there is a compensating mechanism for the decreasing doppler width, the loading rate can be increased. This can be accomplished by either chirping the laser frequency (details can be found in reference [77]), or by using Zeeman effect (as shall be explained later). By chirping the frequency of the counter-propagating laser beam being used for slowing the atoms, a pulsed source of cold atoms can be produced. However, a pulsed source might not be ideal for most experiments.

If the frequency spectrum of the laser cooling beams is broadened by for example, generating side-bands using an electro-optical modulator, the number of trapped atoms can be increased by over 20 fold. Details of such an experimental scheme for ^{7}Li atoms is described in [5]. The side-bands thus created enable the laser to talk to a broader range of velocities, and also (for higher trap-depths) re-capture the decay products of fine-structure changing collisions- thus building up the number of trapped atoms.

4.3.2 Filtering the high velocity atoms

One of the major contribution to trapped atom losses is the collisions of cold atoms with the hotter ones coming from the atomic beam. This could be minimized using two general ways. First, by placing a small beam block in between the source and MOT so that the mostly high velocity atoms don't hit the MOT. The atoms eventually diffuse around and have a smaller average velocity. Also, since the MOT is not in the path of atom beam anymore, the losses due to the high momentum atoms knocking out the cold ones is greatly reduced. This technique is implemented in the photo-association experiment that is being setup in our lab. An example of a beam block placed in front of a source that was very close to the trapping region is given in the experimental setup of [5]. For that particular geometry, loading rates of 10^7 atoms/s were obtained. However, since the source was so close to the MOT, the trap life-time was reduced.

Another possible mechanism relies on the interaction of atoms with high magnetic fields to make a laser-free slow atom source. The atoms are transported through a curved tube that has a octupole magnetic guiding field produced by permanent magnets. Slow, low-field seeking atoms can follow the curved trajectory of the skimmer source, while all other atoms hit the walls of the magnetic guide and are lost. Thus the magnetic guide acts as a low-velocity filter and can lead to around 10^8 atoms in a lithium MOT [31].

4.3.3 Zeeman slower

While these methods described above sacrifice loading rates, they could produce higher steady state numbers. In order to load a high number of atoms quickly (up to 10^{11} atoms/s [79]), a zeeman slower is usually implemented. It uses both interaction with laser and magnetic fields to decelerate an atomic beam to velocities comparable to the capture velocity of the MOT. The following is a simple explanation of the underlying physics. Detailed analysis of the experimental design are described in several Ph.D. theses, including [69]. It is to be noted here that we decided not employ a Zeeman slower, at least initially, because of the technical demands of the slower. However, its working is being briefly described here for completeness.

For a high intensity laser beam, the scattering force on the atom can expressed as [22]:

$$F_{max} = \hbar k \frac{\Gamma}{2} \qquad (4.17)$$

A laser that is counter-propagating to the incoming atomic beam would provide a force that would decelerate the atoms. A moving atom sees the red de-tuned laser beam Doppler shifted to the resonance and absorbs and emits it, eventually losing forward momentum, and slowing down. However, as the atom slows down, the doppler shift changes and it eventually gets out of resonance. So, we add a compensating magnetic field to provide a spatially varying de-tuning that ensures that the laser remains on resonance with the slowing atom beam. The de-tuning

experienced by the atom can expressed as:

$$\Delta = \Delta_{laser} + \frac{v}{\lambda} - \Delta_B \qquad (4.18)$$

where the first term in the sum corresponds to the de-tuning of the slower laser, the second is the doppler shift and the third corresponds to the de-tuning due to the magnetic field. This de-tuning is given by:

$$\Delta_B = \frac{\mu_B B}{h} \qquad (4.19)$$

To ensure that the atom is resonant with the laser, the magnetic field should be such that:

$$B = \frac{h}{\mu_B}(\Delta_{laser} + \frac{v(z)}{\lambda}) \qquad (4.20)$$

This magnetic field is provided by a series of current carrying coils, with increasing number of turns to get a tapering magnetic field with distance to offset for the decreasing doppler shift of the atoms. The magnetic field is chosen so that atoms from a certain velocity onwards get slowed down. A region of magnetic field works for a certain velocity class of atoms- slowing them a bit. So, a tapering magnetic field moves atoms from one velocity class to lower and lower velocities, and by the time the atoms reach the trapping region, all the atoms below a certain velocity (usually the most probably velocity for the atomic beam) have been slowed to much slower velocities comparable to the capture velocity of the MOT. This greatly enhances the loading rate, since the distribution of velocities is not a broad Maxwellian any more, instead it has a sharp peak around the capture velocity (or the slowed velocity for the slower). However, atoms above the upper-bound of the slower remain unaffected by the Zeeman beam, since they are never resonant with it, and lead to losses in the trapped atoms by colliding with them. In spite of this, Zeeman slowing appears to be the most popular choice for efficient lithium laser cooling.

4.4 Our choice of sources

To conclude the discussion of several types of sources begin used for ultra-cold atom experiments, we shall discuss the ones we chose for our atoms and why.

4.4.1 Rubidium

Alkali metal dispensers seem to be the most popular choice for rubidium source. These are little metal oven containing a salt of the alkali metal required (in our case rubidium), and a strong reducing agent. The reducing agent used in commercial dispensers from SAES getters is SAES St101 (Zr 84%-Al 16%) getter alloy. In addition to reducing the alkali back to its metallic state, St101 also absorbs chemically reactive gases from the device, preventing them from contaminating the alkali metal vapor. By switching the current through the dispensers off, the emission of atomic vapour can be stopped rapidly. Also, they are compact, reliable and cheap- which
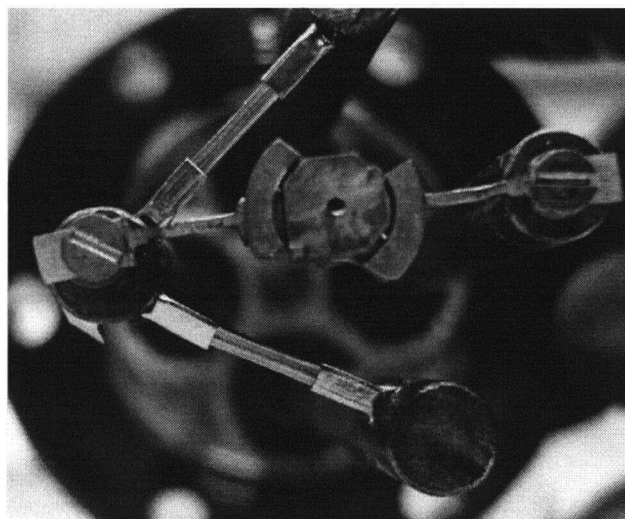
Figure 4.6: Picture of the vacuum system electric feed-through showing the 1/4"
support support rods on which the atomic sources to be used for the experiments
are screwed on. There are two rubidium dispensers on the top and bottom, and a
collimated effusive atomic beam source for lithium is shown in the center.

also contributes to their popularity. In fact loading rates from alkali metal dispensers
have been extensively studied [67]. We decided to use these dispensers in conjunction
with light-induced atomic desorption as demonstrated in [35].

4.4.2 Lithium

Since naturally occurring lithium has only 7.5% ^{6}Li, the rest being ^{7}Li, we got an en-
riched (95%) source of ^{6}Li, since ^{7}Li would be an impurity, and an unnecessary source
of contaminant for our experiment. That also ruled out an alkali metal dispenser as
an atomic source. The low vapour pressure of lithium at room temperature left us
with no choice other than to build an effusive atomic beam source. So, we have a
collimated atomic beam source, combined with a mechanical beam block. A similar
scheme has been demonstrated in lithium already [5]. The technical complexity, and
space considerations associated with a Zeeman slower discouraged us from building
it - however depending on the performance of this source, it might be re-considered.

I shall be telling this with a sigh
Somewhere ages and ages hence:
Two roads diverged in a wood, and I–
I took the one less traveled by,
And that has made all the difference.

The Road Not Taken: Robert Frost

Chapter 5

More IFs: The Vacuum and Control system, and THEN a MOT

If you can keep your head when all about you
Are losing theirs and blaming it on you;
If you can trust yourself when all men doubt you,
But make allowance for their doubting too;
If you can wait and not be tired by waiting,
Or, being lied about, don't deal in lies,
Or, being hated, don't give way to hating,
And yet don't look too good, nor talk too wise..

If: Rudyard Kipling

This chapter is divided into three parts. The first two describe the vacuum and control system respectively. These are two crucial technical aspects of the experiment that have not been addressed so far in this thesis. The third part was added very recently- and shows preliminary data from our Rb and Li MOT.

All experiments with ultra-cold atoms are done in an ultra-high vacuum chamber so that the collision with background gases at room temperature are minimized. Ultra-high vacuum is characterized by pressures lower than 10^{-7} pascal, or 10^{-9} torr. At these temperatures the mean free path of a gas molecule is approximately 40km. So, the chance of collisions is very low. Low vacuum is extremely important for the life-time of the experiment. Quantum degenerate gases won't survive collisions with high momentum residual gas molecules. Also, the steady state number of trapped atoms in a MOT (the starting point of experiments) would be affected by the collisions with background atoms. In the first part of this chapter we shall describe how such a vacuum is obtained in the lab.

Also all experiments with ultra-cold atoms require precise and fast control of the experimental variables. For example turning light off using mechanical shutters, taking images or performing evaporative cooling are some things that require very precise timing, and are performed in time scales of milli-seconds, or even micro-seconds. This prohibits any manual control of the experimental sequence, so an automated control system becomes a necessity. The second part of the chapter describes the most prominent features of the computer control system- the details of it are described in [40] and a future thesis [Keith Ladouceur's masters thesis].

5.1 Vacuum system

5.1.1 Initial considerations

Extreme measures are taken to reach this regime in low pressure. All the assembly is done with proper gloves in order to minimize contaminating the chamber. All materials to be used in vacuum chamber are chosen such that they have very low vapour pressure. This minimizes outgassing from materials, and helps to keep the pressure inside the chamber low. Another source of outgassing is air absorbed on the surface of the vacuum components. A material at room temperature is like a sponge, and many different components of the surrounding air (mostly water vapour) get adsorbed on their surface. When inside the vacuum chamber, these adsorbed materials slowly degas forming what could be thought of as a virtual leak.

In order to drive out these impurities, mostly water and hydrocarbons, all the chamber is assembled and then heated up to as high temperature as possible (somewhere between $200 - 450\ ^0C$) while the chamber is being pumped so that the outgassing materials (including evaporated water) are pumped out.

5.1.2 Vacuum pumps and their limitations

The ultimate pressure attained in a vacuum system depends on the influx of gas as well as the pumping of the gas. The equilibrium pressure is given by the expression [80]

$$p = Q \times (S_p^{-1} + S_i^{-1}) \tag{5.1}$$

Here, Q is the total gas load due to leaks, gassing and connection to other systems, S_p is the speed of the pump (given in liters/second) and S_i is the throughput of the connections of the vacuum system to the pump.

The gas influx can be greatly reduced by a careful choice of materials and optimal design of the vacuum system, the pumping speed is more constricted. Since the volume begin pumped is small (less than 10 liters), modest size commercial pumps with a reasonable pumping speeds are used to attain ultra-high vacuum. It is these connections that generally form the limiting factor for the pressure, and not the pumping speed.

Since there is no cost-effective pump covering the whole pressure range from ultra-high to vacuum[82], a combination of pumps is implemented. We use a turbo pump for the initial pumping during bakeout, followed with an ion pump and a non-evaporable getter (NEG) pump that remain attached to experimental chamber. Here, we shall summarize the different pumps used to get the chamber down to ultra-high vacuum pressures.

Turbo Molecular Pump

A Turbo molecular pump works on the principle that particles can be given momentum in a desired direction by repeated collisions with a moving solid surface For these collisions, it implements a high speed turbine rotor with angles blades such that the

colliding gas molecules are preferentially pumped out of the system creating a vacuum environment [82]. Since its introduction in 1957 [10], turbo molecular pumps have quickly evolved into the workhorse for vacuum technology. The pumping speed for the turbo pump used (Varian V70) is 70 l/s and it performs at typically 80,000 rev/min. We use the turbo pumps during bakeout when very high pumping speed is required to drive out all the degassing materials. After the system is baked, a combination of ion and NEG pump is attached to the experimental chamber.

Ion Pump

The ion pump works in two ways: it removes reactive gases by enabling them to react with freshly deposited reactive metal (such as titanium) and it removes noble gases by ionizing them and then burying the accelerated (by magnetic fields from a permanent magnet) ions on the cathode surfaces. They are best suited for pressures lower than 10^{-5} torr range and are thus turned on after initial pumping by turbo pumps.

First commercial ion pumps followed after the pioneering work done at University of Wisconsin [24]. The commercial system used on the experiment is a Varian Starcell pump with a pumping speed of 20 l/s.

There are two major disadvantages of ion pumps. First, they house strong permanent magnets. Even though they are shielded for most pumps- there is still stray magnetic fields and so it is not advisable to house them very close to the experiment. The other disadvantage is its inefficiency to pump out materials with low chemical reactivity, for example the noble gases and some hydrocarbons like methane.

Non-Evaporable Getter

A non-evaporable getter pump seems to overcome some of the problems with ion pumps in order to achieve low pressure. After being activated by heating, the highly reactive getter material (usually some commercial alloy) adsorbs active gas molecules on its surface by chemical reactions. Heating the getter in vacuum diffuses the passive layer into the bulk of the getter material, thus re-activating it. Since it is devoid of any vibrating or high magnetic field parts, it can be put arbitrarily close to the experimental chamber. Also such getter pumps are efficient in pumping water and hydrogen (typically over 100 l/s)- two of the major contaminants in most vacuum systems. Our experimental chamber employs a SAES getter CapaciTorr pump.

Table 5.1 summarizes some of the important features of the three pumps being used.

Table 5.1: Information about the different vacuum pumps being used.

Pump	Manufacturer/Model	Principle of operation	Pumping speed
Turbo	Varian Turbo V70	high speed turbine rotor	70 l/s
Ion	Varian StarCell	getter + ionization	20 l/s
NEG	SAES CapaciTorr	activated getter material	>100 l/s for H, H_2O

5.1.3 Vacuum bakeout procedure

The importance of baking the entire vacuum chamber

It can be shown that a temperature change of 20 ^{0}C may be expected to increase the pressure of condensed or adsorbed molecules by a factor of 10 [81]. By changing the temperature of the the vacuum system by about 200 ^{0}C, the partial pressures increase by a factor of 10^5. From this it may be concurred that pumping for a second at this high temperature would remove as much gases from the system as pumping for a whole day at room temperature. However, this is not entirely true since there are limitations imposed by the pumping speed of the vacuum pumps involved. However, prolonged baking at high temperatures of the entire vacuum system ensures that we get rid of all the contaminants much faster. It is important to bake the entire vacuum system together because otherwise the molecules condense on the colder parts of the system, and remain as a slowly outgassing source. Figure 5.1 shows the effect of an increase in temperature over pressure of the vacuum system. It can be seen that the pressure first increases, and then over time decreases to a much smaller value.
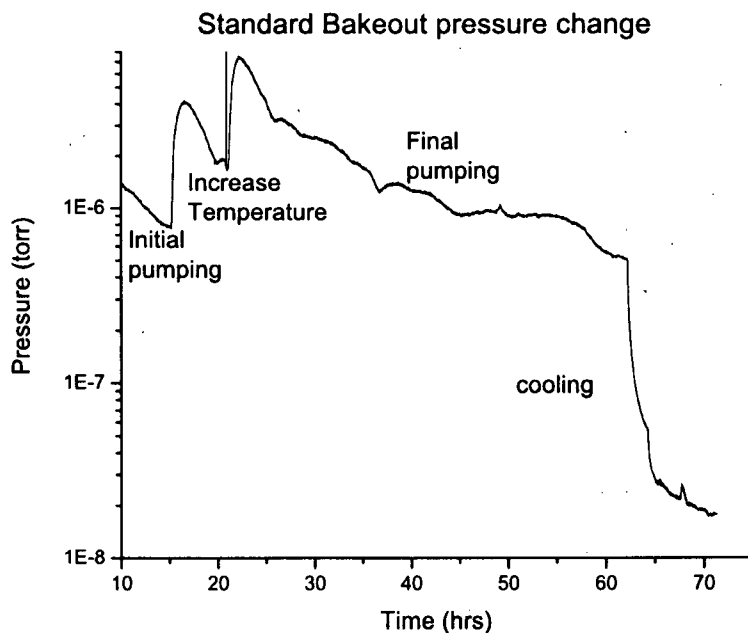

Figure 5.1: Figure illustrating part of the actual lab bakeout procedure. During an increase in temperature, the pressure increases considerably, but over a period of time, the impurities are pumped out, and the base pressure actually decreases considerably after cooling.

The standard procedure for bakeout followed in the lab is being described here.

This could serve as a guideline for future experiments.

Cleaning procedure

The following is the lab standard cleaning procedure for ultra-high vacuum components:
1. 30min in the ultrasonic with detergent (alconox)
2. 15min (once or twice) in the ultrasonic in distilled water for rinsing
3. 15min (once or twice) in the ultrasonic in methanol
4. 15min (once or twice) in the ultrasonic in acetone
It is noteworthy that acetone the highest vapor pressure (compared to other often used organic solvents), so if any of it is left over it will evaporate more quickly.

High temperature air bake

All stainless steel components (including mounting components) are laid separately and baked in the home-built oven up to $400 - 450\,^{0}C$ for 3-4 days in order to drive out all the impurities, mainly consisting hydrocarbons. This is to ensure that most of the impurities have been driven off the surfaces.

Assemble and check parts

After the air bake, the vacuum components are then carefully assembled together (without the still unbaked glass parts and valves), and checked for any leaks by inserting helium gas and looking at a Residual Gas Analyzer (SRS-200 RGA). Any leaking components are replaced.

Preliminary bake

The assembled vacuum system (including the atomic sources, but without the glass cell and NEG pump) is baked at $200\,^{0}C$ for a few (5-10) days. At this point, the atomic sources are turned on and checked. This process also degasses them.

Final bake

With all the pumps connected, and the glass cell on, the entire system is baked at around $200\,^{0}C$ for over a week.
The final pressure obtained for the photo-association chamber, that was baked using these guidelines was better than 10^{-8}torr. Our ion gauge (the pressure measurement device) is not so efficient at these pressures. However, measurements of lifetime of trapped atoms can give a better indication of the vacuum pressure, but they have not been done yet.
Figure 5.2 shows a schematic diagram of the experimental setup, indicating the placement of various components.
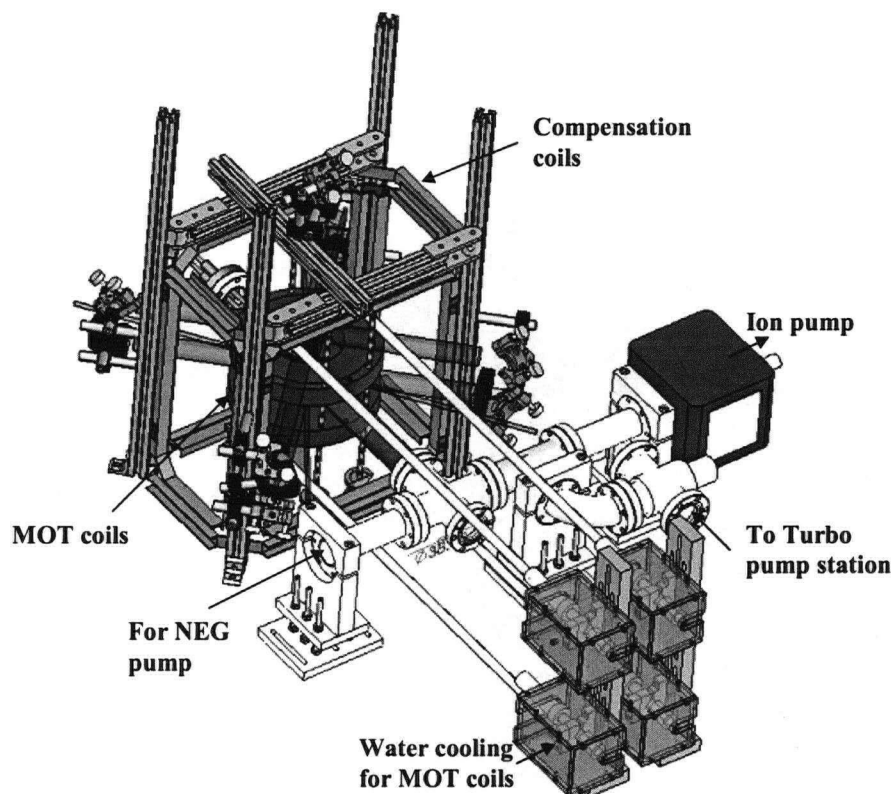
Figure 5.2: Solidworks drawing of the experimental arrangement for Feshbach experiment showing the vacuum system and placement of some optics.

5.2 Computer Control System

5.2.1 Initial considerations

The linear sequence of events that occur while performing experiments with ultra-cold atoms can be automated using standard data acquisition systems. The objective of the effort in our lab is to create a platform independent (independent of operating system) control system that would only require a network connection. This would enable us to do experiments while not really being in the lab. Another important motivation for such a system is the ability to automate optimization of experimental configuration as part of a feedback system, for example, dynamically change detuning of an AOM till the ultra-cold sample has the maximum number of atoms. This saves the experimentalist a lot of time and effort that is put in optimizing the data obtained for every experiment. In the following subsection, I shall give an overview of the components that form part of the computer control system, and the up-to-date progress made on the project.

5.2.2 Hierarchy of components

Base Level Devices

These are the devices that are actually programmed to execute a certain set of instructions. For example the Data Acquisition Card (DAQ). We have a DAQ from National Instruments (NI).

Intermediate Level Devices

These devices are used to convert the input instructions to actual input signals for the instrument in question. For example, a Direct Digital Synthesizer (DDS) is used to get an arbitrary sine wave for input to an AOM. Analog and Digital Output devices that are used to turn the shutter or camera on or off are further examples of such devices.

High Level Devices

These are the devices that perform the actual task during the experiment, for example AOM or optical shutters, or a CCD camera.

5.2.3 The flow of instructions

The experimental recipe is written in python. The user interacts with a graphical user interface to change the experimental sequence as desired. This recipe is converted in to byte code that goes into the NI-DAQ driver buffer. The buffer ensures that the card has information at the right time. This byte sequence is sent to the the UT bus driver that basically changes the 64 pin input from the NI-DAQ card to a 50 pin output. The output of the UT bus goes to the intermediate level instruments like the DDS or Digital output box. These then generate signals for the instruments. It is to be kept in mind that the UT bus can only talk to one instrument at a time, so the time delay in signals should be kept in mind. Figure 5.3 shows the flow of instructions in a flowchart format.

5.2.4 Control software

The software for encoding the NI-DAQ is being written in python and is still under construction. The user shall interact with the graphical user interface of a python script and input the experiment recipe. The python script would code the user commands in to the NI-DAQ input- just a string of 0s and 1s. From here it goes in to the UT bus and then to the devices.

The control sequence so far has been a write only sequence with no inputs being taken. However, one could envision the program to be easily modified to read some input from an oscilloscope, for example over GPIB, and accordingly modify the input control sequence, thus forming a feedback system to optimize certain experimental parameters.
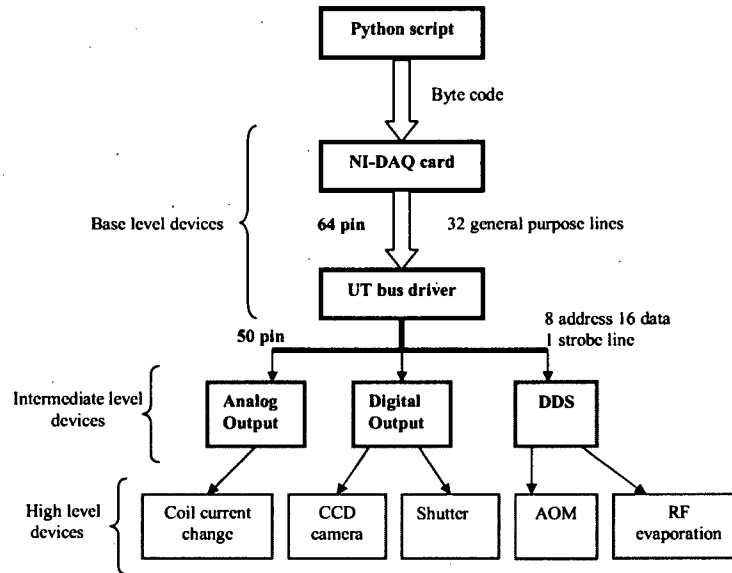
Figure 5.3: Flowchart showing the the sequence in which control instructions are transmitted through the various devices.

5.3 THEN the MOT works

5.3.1 Preliminary fluorescence data

In order to measure the fluorescence of the MOT, we need to consider three quantities: the solid angle of the detector and the scattering rates of the photo-diode and atoms. The number of atoms can be expressed as:

$$N = \frac{\Gamma_{PD}}{\Gamma_{MOT}\eta} \tag{5.2}$$

Here, Γ are the rate of photon emission from a single atom in a MOT (Γ_{MOT}) and the photo-diode detection rate (Γ_{PD}), and η defines the ratio of the fluorescence incident on the detection optics. We shall discuss each one of them separately. Since this calculation estimates the number of atoms roughly, we shall not consider the errors in order to get this ball-park number of atoms.

η is the ratio of the area of the sphere of radius being the distance between detector lens and MOT, and the area of the circular lens.

$$\eta = \frac{\pi a^2}{4\pi D^2} \tag{5.3}$$

Here, a is the radius of the lens and D is the distance between the MOT and the lens. We determined it to be 0.0272 for our geometry.

After making sure that the detector is in the linear regime of operation, we calibrated

the detector to get the optical power detected for the corresponding voltage. The expression was found to be:

$$Power(nW) = -\frac{V}{0.038} \qquad (5.4)$$

Here, V is the negative voltage detected by the photodiode. A background voltage may be added to this expression depending on the value of background during an experiment. Dividing this power by the the energy of each photon (hc/λ), we get the number of photons detected per second. We also take into account 4% losses at the glass surfaces of the uncoated MOT cell and lens. Adding all these, we get the following expression for the photon detection rate.

$$\Gamma_{PD} = 1.21 \times 10^{11}(-V) \qquad (5.5)$$

It is necessary to subtract the background voltage from the quantity in parenthesis in order to get non-negative number of atoms.

The MOT scattering rate, Γ_{MOT} is the number of photons scattering by a single atom in a MOT. As explained in chapter 2, it can be expressed as:

$$\Gamma_{MOT} = \frac{\Gamma}{2}\frac{I/I_{sat}}{1 + I/I_{sat} + (\frac{2\delta}{\Gamma})^2} \qquad (5.6)$$

Here, Γ is the natural line-width. For rubidium, it is equal to 2π 5.9 MHz. The saturation intensity of for rubidium MOT transition is 3.58 mW/cm^2. For 2 mW in each of the six MOT beams with a beam waist of 1 cm, the total intensity at the center of the MOT is 15.3 mW. The ratio of incident intensity to the saturation intensity, also known as the saturation parameter, was thus found to be 4.268. The de-tuning was measured to be $\delta = 9$ MHz for this set of measurements. Putting in all these values, we get the Γ_{MOT} to be 1.435×10^7 photons/s.

This leads to a formula to convert the photodiode voltage to the number of trapped atoms.

$$N = 3.11 \times 10^5(-V) \qquad (5.7)$$

Here B is the background voltage. Figure 5.4 shows a typical loading curve- the number of trapped atoms as a function of time under these parameters for a ^{87}Rb MOT.

5.3.2 Analysis of loading rate

In this sub-section, we shall analyze the loading curve shown in Figure 5.4 to get information about the lifetime and vacuum of the system. The data is fitted to a function of the form:

$$N = A(1 - e^{-k(t-t_0)}) \qquad (5.8)$$

By comparing the fitting function to the expression for loading from a background vapour as mentioned in chapter 4, we see that A is the ratio of loading rate (R) and loss rate (γ). Also, k in the exponential gives the loss rate γ. The trap life-time is
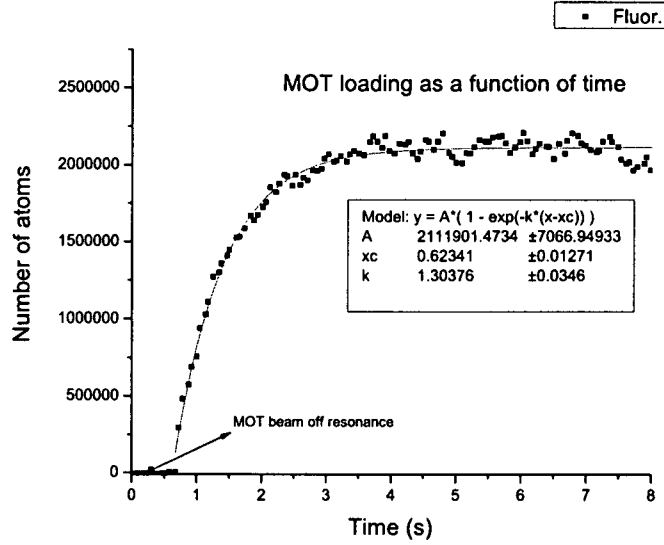
Figure 5.4: Loading rate as a function of time for Rb-87 MOT. Injection to a slave beam was blocked in order to get the background due to non-resonant light. Once unblocked, the light was on resonance, and the MOT started loading.

just the inverse of loss rate, $\tau = 0.79\ s$. From the loss rate, the density of background gas can be extracted.

$$n = \frac{\gamma}{\sigma v_{mp}} \tag{5.9}$$

For a gas of rubidium atoms at room temperature, and collisional cross-section of $6.3 \times 10^{-13}\text{cm}^2$, we get density n to be $8.35 \times 10^7\text{atoms/cm}^3$. From ideal gas law, we get the corresponding pressure to be 2.6×10^{-9} torr.

It is an interesting exercise to use the value of number density we obtained to calculate the loading rate of the MOT from background vappour and compare it to our model's loading rate. The expression for loading rate is given by:

$$R = \frac{nV^{2/3}v_c^4}{2v_{mp}^3} \tag{5.10}$$

Using our experimental parameters (de-tuning, which gives the capture velocity, v_c and the MOT area, V), we get the loading rate to be 7.67×10^4 atoms/s. This is significantly lower than the loading rate obtained from fitting the data to our model, which gives us a loading rate of 1.68×10^6. This is because our atomic source is actually an effusive source, the alkali dispenser, and not just background vapour. These measurements were obtained shortly after turned the dispensers off, and that is the reason for the higher loading rate.

It is important to note that the loss rate determined here only considers collisional

losses with background rubidium. There are other loss mechanisms. For example, there are losses due to collision with other atoms as well as light assisted collisional losses that is not being considered here. So, the number of atoms is an over-estimate. Figure 5.5 is a picture of another ^{87}Rb MOT. Around 10^9 were trapped in this first MOT. Since the detectors have not yet been calibrated for lithium, and the number of atoms is being optimized, no useful data has been obtained on the lithium MOT. However work is under progress, and useful measurements characterizing the performance of the MOT are under way.
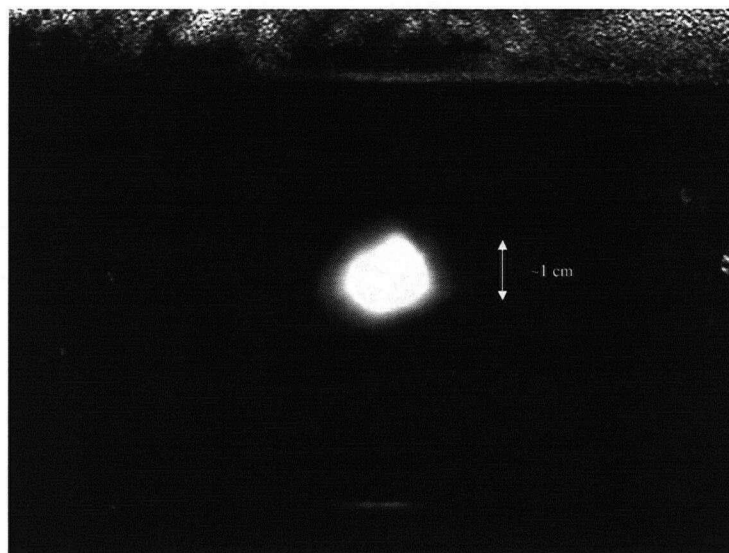

Figure 5.5: Picture of around 10^9 fluorescing ^{87}Rb atoms in a MOT taken on April 13th, 2007. The lithium atom also works, however, it needs more calibration and optimization.

If you can fill the unforgiving minute
With sixty seconds' worth of distance run -
Yours is the Earth and everything that's in it,
And - which is more - you'll be a Man my son!

If: Rudyard Kipling

Chapter 6

Towards hetero-nuclear molecules and Quantum Degenerate Gases

Old Walt Whitman
Went finding and seeking,
Finding less than sought
Seeking more than found,
Every detail minding
Of the seeking or the finding

Old Walt : Langston Hughes

This chapter describes the research goals of the group. Currently there are three experiments with ultra-cold atoms. Figure 6.1 shows a schematic diagram with the major technical and scientific goals of these experimental initiatives. This chapter briefly describes the different experiments being built, the motivation and their progress. Since the work of this thesis was primarily done on building the feshbach resonances and quantum degenerate gases experiment, it will be emphasized.

6.1 Miniature Atom Trap

The primary goal of this experiment is to develop techniques to enable miniaturization and portability of atom-chip based devices. Ultra-cold atoms have led to several advancements in precision measurements- for example the development of atomic fountain clocks and precise measurements of atom-surface interactions. However, since the experimental chamber is not portable and small, it prohibits larger scale development of this technology.
Portable ultra-high vacuum chambers have already been demonstrated [39]. Trapping atoms using magnetic fields from wires on a silicon surface close to the atomic cloud has also been demonstrated in several laboratories [66]. By combining these techniques and developing a few others, a miniature chip package that is robust and portable can be envisioned. This is the primary goal of this experiment, which is being done in collaboration with Dr. James Booth from British Columbia Institute of Technology.

6.2 Ultra-cold heteronuclear molecules

As eluded to in the first chapter of this thesis, atomic physics is moving beyond ultra-cold atoms towards observation of many-body phenomenon that is characterized by
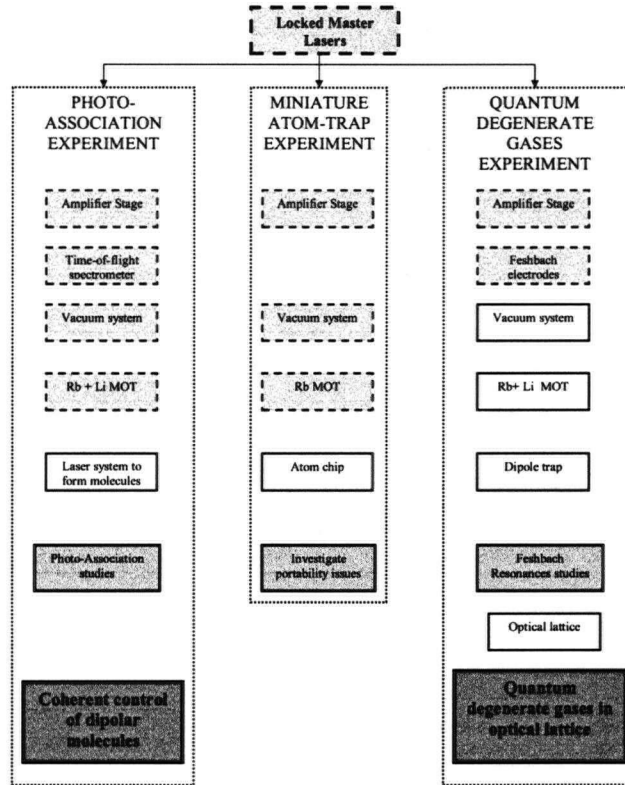
Figure 6.1: Schematic diagram showing the objectives of the experimental effort. The dashed boxes are technical goals that have already been accomplished. The filled dark boxes represent the short and long term research goals.

strong interactions between atoms. The creation of an ultra-cold sample of molecules with an intrinsic dipole moment, such as alkali dimers of two different atoms, provides a sample with anisotropic interactions. Combined with the precise control and tunability provided by techniques of ultra-cold experiments, these may lead to advancement of current efforts in several fields including quantum computing [27] or BEC of dipolar gases [46] to name a few. Perhaps even more interesting is the unexplored physics that awaits- for example, topological quantum states[78], super-solid order[12] or phase separation [60]. There is also the possibility of occurance of new phenomena that has not yet been anticipated.

So far, there are two demonstrated methods for creating ultra-cold polar molecules from ultra-cold atoms. First is via photo-association, where a laser beam excites atoms to form a hetero-nuclear molecule in its electronically excited state (for example see [61]). These molecules eventually decay into the ground state. The goal of the photo-association experiment is to create molecules using this method and then investigate schemes to drive them into their lowest ro-vibrational state using Raman transitions. Ultra-cold molecules in their absolute ground state are required to observe several of the phenomenon referred to in the previous paragraph. The details

of this experiment would be described in a future thesis [Nina Rauhut and Bastian Schuster diploma thesis]. Another method to create ultra-cold molecules involves the use of Feshbach resonances. This approach will be described in detail in the following sections.

6.3 Feshbach resonances

The properties of a gas of ultra-cold atoms are described in terms of a very important parameter, the s-wave scattering length a_s. At ultra-cold temperatures, when the two-body collision processes dominate the dynamics of the atomic sample, both elastic and inelastic collisions depend on the singlet and triplet channel's s-wave scattering length.[83] This parameter a determines the thermalization rate, stability and mean-field energy of a quantum-degenerate gas[22].

In the recent years, we have seen a revolution in atomic physics, which is lead by the observation of Feshbach resonances in ultra-cold alkali atoms. Feshbach resonances provide the experimental knob to tune the interactions in these atomic samples from positive infinity to negative infinity. The scattering length, a_s, can be tuned using magnetic fields. The resonance occurs when a bound state in a higher energy "closed" molecular channel becomes degenerate with the collision energy along the "open" inter-atomic channel, as shown in Figure 6.2.
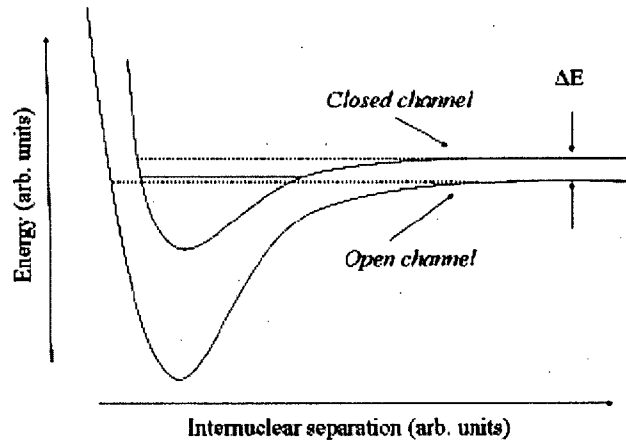
Figure 6.2: Schematic diagram explaining a feshbach resonance. The upper bound state gets degenerate with the collision energy of the input channel.(Figure from [57])

Since the first observation of feshbach resonances in a BEC [36], these resonances have been used to enable controlled collapse of a BEC [62], ultra-cold diatomic molecules[30] and the realization of the BEC-BCS crossover in the ultra-cold neutral atom system[16] to name a few phenomenon. On a more relevant note, Feshbach spectroscopy can be used to precisely determine the interatomic interaction potential,

often to an unprecedented level of accuracy, and molecular structure near dissociation [17]. Determination of lithium-rubidium interatomic potential via photo-association and feshbach spectroscopy is one of the primary scientific goals of the laboratory.

While Feshbach resonances in homonuclear molecules have been studied extensively, not much work has been done (either experimentally or theoretically) on Feshbach resonances between two different atomic species. Nevertheless, such resonances have been observed in a $^6Li - ^{23}Na$ system [17] and $^{40}K - ^{87}Rb$ system[68]. But there are several other atomic species that remain unexplored. The goal of this research project is to estimate the location and widths of such s-wave Feshbach resonances in $^6Li - ^{87}Rb$ system.

In comparison to homonuclear molecules, the Feshbach spectrum of heteronuclear molecules is richer. This is because the hyperfine constants are unequal for the two atoms and there are four rather than three zero-field collision asymptotes[57]. Also, these two-species feshbach resonances are the first step towards the study of a Bose-Fermi mixture with tunable interactions, a field that could lead to another revolution in ultra-cold physics. Some of the predicted possibilities include the formation of ultra-cold polar molecules with phase-space densities much higher than that obtained by photo-association, which might lead to interesting physics in the quantum degenerate regime.

6.3.1 Experimental Strategy

A dual species MOT will be created to trap both ^{6}Li and bosonic Rubidium isotopes, ^{85}Rb or ^{87}Rb. Here the magnetic coils are set to produce a quadrupole magnetic field by using inverse current in the upper and lower coils. The current flow is about 2A which can provide a 10 Gauss/cm magnetic field gradient for our dual species MOT. Once the atoms are cooled by the dual species MOT, an optical tweezer will be used to trap these atoms for later Feshbach resonance experiment. The optical tweezer is created by a 10 mW CW Yb Fiber laser with center wavelength 1064 nm and linewidth <100kHz, after amplified by the Yb Fiber amplifier, it will give a 20W CW saturated output power. A resonance cavity will be used to enhance the optical dipole trap [3].

After the atoms are trapped by the optical tweezer, the magnetic coils are changed to Helmholtz coils, which provides a uniform magnetic field between the coils. The current here will be 10 A to 25 A and will produce a uniform magnetic field between 500 and 1000 gauss. After allowing the ensemble to evolve for some time at a specific magnetic field, the temperature and the number of trapped atoms will be measured by shining Lithium and Rubidium resonant lasers into the optical trap after extinguishing the external field.

As described before, the presence of a Feshbach resonance is characterized by loss in the number of atoms due to formation of molecules and a divergence in the collisional cross-section, and hence faster thermalization rates. By checking the relationship between the decay rate of the number of trapped atoms with corresponding magnetic field intensity, the hetero-nuclear Feshbach Resonances between Lithium and Rubidium can be found. A hetero-nuclear Feshbach resonance would be characterized by

losses in the number of both rubidium and lithium atoms.

6.4 Electric-field-induced Feshbach resonances

So far collisions of ultra-cold atoms have been controlled either by magnetic fields using feshbach resonances, or by lasers using near-resonant light, raman transitions or optical lattices. However, recent theoretical proposals exhibit control of interactions between atoms of two species by tuning DC electric fields [51, 55].

When two different atoms collide, they form a collision complex with an instantaneous dipole moment. This dipole moment function is peaked around the equilibrium distance of the diatomic molecule in its ground vibrational state. The dipole moment enables the collision complex to interact with an external electric field. Electric fields induce couplings between different angular momentum states due to the interaction of the instantaneous dipole moment of the collision pair with external electric fields. Addition of an external electric field hence provides a mechanism to couple the incoming open channel to bound states (closed channel) of different orbital momentum (as opposed to only s-wave bound states provided by feshbach resonances), hence opening a new genre of controlled interactions called electric field induced feshbach resonances. Also, it has been proposed that the electric field couplings could induce new feshbach resonances and shift the position of s-wave magnetic resonances [55].

6.4.1 Experimental Strategy

such resonances have not yet been observed experimentally. Progress is being made to insert DC electrodes providing the desired electric fields of around 100kV/cm (see Figure 6.3) and make an optically trapped sample of atoms interact with it. The optical trap would be made from the 1064 nm CW Yb fiber laser, as described in the previous section. The key here is to position the tweezer using two galvos. in order to optically trap mixture of rubidium and lithium in the presence of the electric field, and then observe losses via absorption spectroscopy in order to detect the presence of Feshbach resonances.

6.5 Quantum Degenerate Gases as quantum simulators

Recent technological developments have made it possible to study rich many body physics using ultra-cold atomic gases trapped in periodic optical potentials as quantum simulators for strongly correlated quantum systems. For example, the Bose-Hubbard model was recently realized with a Rubidium BEC in an optical lattice [58]. The primary goal of the proposed research project is to build an apparatus to prepare an ultra-cold sample of fermionic lithium atoms, trap the atoms efficiently in an optical lattice potential formed by the interference of intersecting laser beams, and measure the properties of the confined gas. The preliminary step is to build a

Figure 6.3: A picture of the high DC voltage electrodes attached to a 1.33" vacuum CF flange electrical feedthrough before being inserted in the vacuum chamber. The spacing between the electrodes at the curved end, where the cold atoms would be inserted is around 1.3 mm.

magneto-optical trap for laser cooling and trapping of the atomic sample and this is currently being carried out as this master's thesis project. After this important step, lithium will be further cooled by elastic collisions with ultra-cold rubidium atoms in order to reach the quantum degenerate regime, where all the experiments will be carried out. Evaporative cooling of spin polarized fermions is hindered because s-wave collisions (the dominant collision channel at ultra-cold temperatures) are not allowed due to Pauli Exclusion Principle. Hence another ultra-cold atomic species is introduced to lower the temperature of the lithium ensemble.

Lithium is a spin 1/2 system in its ground state and it is therefore a natural atomic system for being a quantum simulator for electrons in a lattice. Once the experimental machine is built, several model Hamiltonians of spin 1/2 systems could be studied. In particular, the quantum phases of the so-called Hubbard lattice model [78] will be explored in detail.

6.5.1 The Fermionic Hubbard Model

The Hubbard model was introduced in 1963 to study electron correlations in narrow energy bands [45]. It is the sum of two different hamiltonians, both of which will be described separately here.

The first part of the Hubbard hamiltonian is the hopping term, H_{hop}, which describes the quantum mechanical tunneling of electrons between lattice sites. In second quantized notation, it can be expressed as:

$$H_{hop} = \sum_{x,y \in \Lambda} \sum_{\sigma=\uparrow,\downarrow} t c_{x,\sigma}^{\dagger} c_{y,\sigma} \qquad (6.1)$$

Here, $\uparrow, \downarrow$ denote the two spins, Λ denotes the set of all the lattice sites with x and y being two neighbouring lattice sites, and t is the tunneling amplitude. $c^{\dagger}$ is the particle creation and c is the annihilation operator.

From elementary quantum mechanics knowledge, one can make an assumption that the ground state wavefunction of this hamiltonian is obtained by filling up the lowest

energy levels by $\uparrow$ and $\downarrow$ electrons. This is indeed correct. An important observation would be that the system has a total spin of zero and exhibits no long range order. The electrons simply behave as waves.

The second term in the Hubbard hamiltonian comes from the repulsive interaction between electrons at a lattice site (a simplified version of coulomb energy, which is actually long-range). In second quantized notation, it can be expressed as:

$$H_{int} = \sum_{x \in \Lambda} u_x n_{x,\uparrow} n_{x,\downarrow} \tag{6.2}$$

If the number of electrons is less than the number of lattice sites, the ground state would simply be described by each electron at a different lattice site, being completely oblivious to the presence of another electron, such that the total energy is zero. Again, there is no long-range order and the electrons would fit a simple particle-like description.

The Hubbard model is a simplified description of an interacting fermionic system. It corresponds to the sum of two non-commuting representations- the wave-like picture (demonstrated by H_{hop}) and the particle-like picture (H_{int}) of electrons. However, just like quantum mechanics is enriched by the wave-particle dualism, so is the Hubbard model. Even though each of its constituent hamiltonians do not show any long range order, the Hubbard hamiltonian is believed to generate various non-trivial phenomenon including the metal-insulator transition, anti-ferromagnetism, ferromagnetism and even superconductivity [56, 73].

The search of this model's parameter space continues to be a challenging problem for mathematicians and physicists alike. Several distinct mean-field solutions exist at most points in the model's parameter space. It is possible and even likely that states occur which are not even anticipated at present. Experimental study of many-body fermionic atom systems appears to be the best strategy, at the present time, to decipher the riddles of the fermionic Hubbard model. Using quantum degenerate lithium atoms in an optical lattice as a quantum simulator, this complex many body problem could be addressed, if not solved. The potential impact of this experimental research on both physics and mathematics is immense.

6.5.2 Experimental Strategy

Sympathetic cooling of ^{6}Li in the presence of an evaporatively cooled sample of ^{87}Rb has been demonstrated in a magnetic trap [15]. The inter-species s-wave scattering length was estimated to be $|a_s| = 20^{+9}_{-6} a_B$, where a_B is the Bohr radius. The small value of the inter-species scattering length means that sympathetic cooling dynamics of the mixture is slow. The collision rate is given by the familiar equation:

$$\gamma_{coll} = \sigma_{mix} \bar{v} n_{mix} \tag{6.3}$$

Here, the collisional cross-section is given by $\sigma_{mix} = 4\pi a_s^2$, $\bar{v}$ is the mean thermal velocity of the ensemble and n_{mix} is the the overlap density of the two atomic clouds. The thermalization rate is given by [15]:

$$\gamma_{therm} = \xi \gamma_{coll}/2.7 \tag{6.4}$$

Here, ξ is the reduction factor due to the unequal masses of the two species, and is given by:

$$\xi = \frac{4m_6 m_{87}}{(m_6 + m_{87})^2} \tag{6.5}$$

The temperature difference between the two clouds evolves as:

$$\frac{d}{dt}(\Delta T) = -\gamma_{therm}\Delta T \tag{6.6}$$

As the rubidium cloud is cooled evaporatively, the lithium cloud also decreases in temperature due to this thermalization. It is to be noted that the inter-species scattering length plays an important role in the time-scales associated with this process. By tuning this parameter via a Feshbach resonance, the thermalization rate can be greatly enhanced and the phase space density of lithium increased due to the subsequent decrease in temperature. This ties the investigation of Feshbach resonances between rubidium and lithium with the search for novel routes to quantum degeneracy in ensembles of ultra-cold atoms. With the atoms being trapped in an optical trap to reduce inelastic collisional losses associated with the feshbach resonance and two different istopes of rubidium being investigated ^{87}Rb and ^{85}Rb, this approach certainly appears promising.

Pleasured equally
In seeking as in finding,
Each detail minding,
Old Walt went seeking
And finding

Old Walt : Langston Hughes

Bibliography

[1] W I. McAlexander G. B. Partridge A. G. Truscott, K. E. Strecker and R. G. Hulet. *Science*, 291(5513), 2001.

[2] P. Eugster A. Keshet. The story of a laser. Technical report, QDG Lab, Physics dept. UBC, Aug 2005.

[3] H. Moritz T. Elssser M. Weidemller A. Mosk, S. Jochim and R. Grimm. *Opt. Lett.*, 2001.

[4] C.S. Adams and E. Riis. *prog. Quant. Electr.*, 21(1):1, 1987.

[5] B.P. Anderson and M.A. Kasevich. *Phys. Rev A.*, 50:R3581, 1994.

[6] B.P. Anderson and M.A. Kasevich. *Phys. Rev A*, 63:023404, 2001.

[7] J.F. Annett. *Superconductivity, Superfluids and Condensates.* Oxford University Press, 2004.

[8] J.S. Wilson A.S. Arnold and M.G. Boshier. *Rev. Sci. Instrum.*, 69:1236, 1998.

[9] A. Ashkin and J.P. Gordon. *Optics Letters*, 8(10):511, 1983.

[10] W. Becker. *Vak. Tech.*, 7:149, 1958.

[11] G. C. Bjorklund and M. D. Levenson. *Appl. Phys. B*, 32:145, 1983.

[12] H.P. Buchler and G. Blatter. *Phys. Rev. Lett.*, 91(130404), 2003.

[13] K. P. Weber C. J. Hawthorn and R. E. Scholten. *Rev. Sci. Instrum.*, 72(12):4477, 2001.

[14] H. Robinson C.E. Wieman C. Monroe, W. Swann. *Phys. Rev. Letters*, 65(4):1571, 1991.

[15] C. Marzok B. Deh Ph.W. Courteille C. Silber, S. Gu nther and C. Zimmermann. *Phys. Rev. Lett.*, 2005.

[16] M. Greiner C.A. Regal and D.S. Jin. *Phys. Rev. Lett.*, 92(040403), 2004.

[17] C.H. Schunck S.M.F. Raupach C.A. Stan, M.W. Zwierlein and W. Ketterle. *Phys. Rev. Lett.*, 93(143001), 2004.

[18] M.E. Carrera-Patino and R. Stephan Berry. *Phys. Rev. A*, 34(6):1, 1986.

[19] D. Cassettari. *Cold Atoms in Microscopic Traps: From Wires to Chips.* PhD thesis, Innsbruck, 2000.

[20] L. Hollberg C.E. Wieman. *Rev. Sci. Instrum.*, 62(1):0001, 1991.

[21] L. Hollberg C.E. Wieman. *PRA*, 72(043409), 2005.

[22] H. Smith C.J. Pethik. *BEC in dilute gases.* Cambridge University Press, 2002.

[23] J. Dalibard and C. Cohen-Tannoudji. *J. Opt. Soc. Am. B*, 6(11), 1989.

[24] R.H. Davis and A.S. Divatia. *Rev. Sci. Inst.*, 25:1193, 1954.

[25] L. de Broglie. *Comp. Rend. Ac. Sci*, 177:507, 1923.

[26] B. DeMarco and D.S. Jin. *Science*, 285:1703, 1999.

[27] D. DeMille. *Rev. Sci. Instrum.*, 88(067901), 2002.

[28] M.Inguscio E. Arimondo and P.Violino. *Rev. of Mod. Phys.*, 1:31, 1977.

[29] S. Chu E. Raab M. Prentiss, A. Cable and D. Pritchard. *Phys. Rev. Lett.*, 59:2631, 1987.

[30] S.T. Thompson E.A. Donley, N.R. Claussen and C.E. Weiman. *Nature*, 417(529), 2002.

[31] B. Ghaffari et al. *Phys. Rev A.*, 60:3879, 1999.

[32] Boshier et al. *Opt. Commun.*, 85:356, 1991.

[33] M.H. Anderson et al. *Science*, 269:198, 1995.

[34] P.D. Lett et. al. *J. Opt. Soc. Am. B*, 6(11):2084, 1989.

[35] S. Aubin et al. *J. of low T. Phys.*, 140:377, 2005.

[36] S. Inouye et al. *Nature*, 392(151), 1998.

[37] R.P. Feynman. *Foudations of Physics*, 16(6):507, 1986.

[38] C.J. Foot. *Atomic Physics.* Oxford University Press, 2005.

[39] C. Boragno G. Firpo, F. Buatier de Mongeot and U. Valbusa. *Rev. Sci. Instrum.*, 76(026108), 2005.

[40] Raymond Meng Gao. Zoinks and z.759 - the unfinished computer experimental control system. Technical report, QDG Lab, Physics dept. UBC, Aug 2005.

[41] G.R. Hadley. *IEEE Quantum Electron.*, QE-22:419, 1986.

[42] T.W. Hansch and Schawlow. *Opt. Comm.*, 13:68, 1975.

[43] K.C. Harvey and C.J. Myatt. *Opt. Lett.*, 16:910, 1991.

[44] K. Huang. *Introduction to Statistical Physics.* taylor and Francis, 2001.

[45] J. Hubbard. *Proc. Royal Soc. (London)*, 1963.

[46] T. Koch M. Fattori T. Pfau S. Giovanazzi P. Pedri J. Stuhler, A. Griesmaier and L. Santos. *Phys. Rev. Lett.*, 2005.

[47] J.J. Clarke B. Lu J. Walls, R. Ashby and W.A. van Wijngaarden. *Eur. Phys. J. D*, 22:159, 2003.

[48] M. Kasevich and S.Chu. *PRL*, 69(12):1741, 1992.

[49] S. Kasapi K.E. Gibble and S. Chu. *Opt. Lett.*, 17:526, 1992.

[50] W. Ketterle, D.S. Durfee, and D.M. Stamper-Kurn. Making, probing and understanding bose-einstein condensates, 1999.

[51] R. Krems. *Phys. Rev. Lett.*, 96(123202), 2006.

[52] H.G. Kuhn. *Atomic Spectra.* Academic Press, 1969.

[53] S. L. Moi, S. Gozzini and C. Gabbanini, editors. *Light induced kinetic effects on atoms, ions and molecules*, 1991.

[54] M.D. Levenson. *Introduction to non-linear laser spectroscopy.* Academic Press, 1982.

[55] Z. Li and R. Krems. *Phys. Rev. A*, 75(032709), 2007.

[56] E.H. Lieb. The hubabr model: some rigorous results and open problems, 1993.

[57] S.B. Weiss M. Bhattacharya, L.O. Baksmaty and N.P. Bigelow. *Eur. Phys. J. D*, 31(301), 2004.

[58] T. Esslinger T. W. Hansch M. Greiner, O. Mandel and I. Bloch. *Nature*, 415:39, 2002.

[59] H.J. Metcalf and P. van der Straten. *Laser Cooling and Trapping.* Springer, 1999.

[60] K. Molmer. *Phys. Rev. Lett.*, 80:1804, 1998.

[61] A. R. L. Caires V. S. Bagnato M.W. Mancini, G. D. Telles and L.G. Marcassa. *Phys. Rev. Lett.*, 92(133203), 2004.

[62] S.T. Thompson N.R. Claussen, E.A. Donley and C.E. Wieman. *Phys. Rrev. Lett.*, 89(010401), 2002.

[63] F.A. van Abeelen P. Courteille, R.S. Freeland D.J. Heinzen and B.J. Verhaar. *Phys. Rev. Lett.*, 81:69, 1998.

[64] J.H. Eberly P.W. Milonni. *Lasers*. John Wiley and Sons, 1988.

[65] Y.B Ovchinnikov R. Grimm, M. Weidemller. *Rev. Sci. Instrum.*, 42:95, 2000.

[66] Donatella Cassettari Bjrn Hessmo Thomas Maier Ron Folman, Peter Krger and Jrg Schmiedmayer. *Phys. Rev. Lett.*, 84:4749, 2000.

[67] L. Consolino L. Pappalardo N. Marino G.D'Arrigo S. Bartalini, I. Herrera and F.S. Cataliotti. *Eur. Phys. J. D*, 36:101, 2005.

[68] M.L. Olsen C.Ticknor J.L. Bohn S. Inouye, J. Goldwin and D.S. Jin. *Phys. Rev. Lett.*, 93(183201), 2004.

[69] T.A. Savard. *Raman Induced resoance imaging of trapped atoms*. PhD thesis, Duke University, 1998.

[70] R. Shankar. *Principles of Quantum Mechanics*. Plenum, 1994.

[71] S.L. Shapiro and S.A. Teukolsky. *Black Holes, White Dwarfs and Neutron Stars, The Physics of Compact Objects*. Wiley, 1983.

[72] I.I. Sobel'man. *Introduction to the theory of Atomic Spectra*. Pergamon Press, 1972.

[73] H. Tasaki. *J. Physics: Cond. Matt.*, 1998.

[74] L. Valyi. *Atom and Ion Sources*. John Wiley and Sons, 1977.

[75] S.J. van Enk and G. Nienhuis. *Phys. Rev. A*, 46(3):1438, 1992.

[76] J.T. Verdeyen. *Laser Electronics*. Prentice Hall, 1989.

[77] J.L. Hall W. Ertmer, R. Blatt and M. Zhu. *Phys. Rev Lett.*, 54:996, 1985.

[78] P. Zoller E. Demler W. Hofstetter, J.I. Cirac and M.D. Lukin. *Phys. Rev. Lett.*, 89(220407), 2002.

[79] M.A. Joffe A. Martin W. Ketterle, K.B. Davis and D.E. Pritchard. *Phys. Rev. Lett.*, 70:2533, 1993.

[80] M. Weidemller and C. Zimmermann, editors. *Interactions in Ultracold Gases*. Wiley, 2003.

[81] G.L. Weissler and R.W. Carlson, editors. *Methods of Experimental Physics: Vacuum Physics and Technology*. Academic Press, 1979.

[82] G.F. Weston. *Ultra-high Vacuum Practice*. Butterworths, 1985.

[83] W.C. Stwalley W.T. Zemke. *J. Chem. Phys.*, 114(10811), 2001.

[84] A. Yariv. *Quantum Electronics*. John Wiley and Sons, 1989.

[85] Cunyun Ye. *Tunable External Cavity Diode Lasers*. World Scientific, 2004.

Appendix A

Broadening Mechanisms in Atomic spectra: Appearance and Reality

Is there any knowledge in the world which is so certain that no reasonable man would doubt it?

Chapter 1- "Appearance and Reality"
The Problems of Philosophy: B. Russell

The following is a discussion of different kinds of mechanisms that are responsible for the broad spectral line shapes that we observe in the lab. It is important to understand their origin and how much they affect the spectrum, i.e. what is the frequency broadening of the transition caused by them. The elimination, or at least suppression of certain broadening mechanisms will also be discussed.

A beam of N photons (or any particle for that matter) propagating along z in a scattering medium will lose particles as

$$dN(z) = -N(z)p(z)dz \tag{A.1}$$

where $p(z)$ is the probability per unit length of a scattering event and is given by

$$p(z)dz = n_0\sigma dz \tag{A.2}$$

where n_0 is the spatial density of scatterers and σdz is the cross-sectional volume swept out by the moving particle. Since the probability of absorption is equal to the fraction of intensity lost during absorption, we can think of this intensity fraction as

$$\frac{dI}{I} = -n_0\sigma\Delta z \tag{A.3}$$

Attenuation of a beam per unit distance can be described as:

$$\frac{dI}{dz} = -n_0\sigma I \tag{A.4}$$

let us define a quantity that characterizes absorption and call it absorption coefficient, a, such that

$$\frac{dI}{dz} = -a(\omega)I \tag{A.5}$$

Integrating the expression, we get the exponential decay in intensity as a function of distance.

$$I(\omega, z) = I(\omega, 0)\exp{-a(\omega)z} \tag{A.6}$$

for a two-level system in the presence of intense laser radiation, stimulated emission must be taken into account Thus, n_0 gets replaced by $(n_1 - n_2)$, where n_1 and n_2 are the population densities of the ground and excited state respectively. This difference in population densities can be re-written as [38]

$$n_1 - n_2 = \frac{n_0}{1 + I/I_s} \tag{A.7}$$

where I_s is the saturation intensity defines as:

$$I_s = \frac{\hbar \omega A_{21}}{2\sigma(\omega)} \tag{A.8}$$

Here, A_{21} is the spontaneous emission rate for the two level atom. Substituting these results, we get an expression for the absorption coefficient.

$$a = \frac{N\sigma(\omega)}{1 + (I/I_s)} \tag{A.9}$$

This part of the thesis discusses the different mechanisms that contribute to this absorption coefficient, and how it leads to broadening the absorption spectrum.

A.1 Homogeneous and Inhomogeneous mechanisms

Different broadening mechanisms can be classified into two categories: homogeneous broadening, and inhomogeneous broadening. If each atom in the ensemble gets affected the exact same way by the broadening mechanism, it is called homogeneous broadening. Examples of such broadening include natural line width and laser linewidth. If each atom is affected differently by the broadening mechanism, it is called inhomogeneous. A perfect example if this would be Doppler broadening where each atom is affected differently, depending on its velocity. An extensive discussion of the different mechanisms can be found in most laser textbooks, for example, [64]. In the following sections, we shall discuss the different relevant mechanisms that contribute to broadening of our atomic spectra.

A.2 Natural line-width

The idea behind this mechanism is a simple one, and there is a classical analog of this radiative broadening mechanism that I shall mention here (refer to [72] for details). A radiative system loses energy, so free oscillations of such a system must be damped (here comes the damped electron oscillator). But a damped system is not monochromatic, and contains a set of frequencies, and this leads to broadening of spectral lines. From classical electrodynamics, the distribution of intensity in the emission spectrum of an oscillator is described by the dispersion formula:

$$I(\omega) = I \frac{\gamma}{2\pi} \frac{d\omega}{(\omega - \omega_0)^2 + (\frac{\gamma}{2})^2} \tag{A.10}$$

where γ is the damping constant. This leads to the line-width that we observe. Since, we are not scared of quantum mechanics, lets have a closer look at what determines the probability of a photon getting scattered by the atom (Equation A.2).For a photon in an atomic vapor, the absorption cross-section is frequency dependent and given by

$$\sigma = \sigma_0 \frac{\Gamma^2/4}{\delta^2 + \Gamma^2/4} \tag{A.11}$$

where $\Gamma = 2\pi/\tau$ is the atomic line width (τ the excited state lifetime), $\sigma_0 = \lambda^2/2\pi$ is the resonant cross section, and $\delta = \omega - \omega_{atom}$ is the frequency de-tuning of the incident photon from the atomic resonance.

The natural line-width is due to the radiation process itself. If we think of a two-level atomic system, its classical analog can be the damped electron oscillator, and this line-width will be associated with the line width of the oscillator at resonance (this can clearly be seen by comparing equation A.11 to that of a classical oscillator). This classical picture provides a sufficient approximation to the process, especially for the strong S-P transition of alkali atoms. For a more complete treatment of the topic, please refer to reference [52] or [72].

A.3 Doppler broadening

If the atom is moving at a velocity v then it would see the light Doppler-shifted by an amount $k_L v_z$ where $k_L = 2\pi/\lambda$ is the wavevector and v_z is the component of the velocity along the photon beam axis. At a given temperature, an ensemble of atoms have a standard Maxwell-Boltzmann distribution of velocities.

$$n(v_z) \propto n_0 e^{-\beta \frac{1}{2} m v_z^2}. \tag{A.12}$$

If we ignore the natural line-width of the transition (which is negligible compared to this effect anyways), then we would expect the absorption profile to emulate this Maxwellian distribution, and this is what is precisely observed experimentally. Consider that the laser is on resonance and has a negligible line width so that the detuning is simply $\delta = k_L v_z$, and so the density can be written as a function of the velocity dependent detuning as

$$n(\delta) = \frac{n_0}{\sigma_\delta \sqrt{2\pi}} e^{-\frac{\delta^2}{2\sigma_\delta^2}} \tag{A.13}$$

where now $n(\delta)$ is normalized to n_0 and the thermal broadening is given by

$$\sigma_\delta^2 = \frac{k_L^2}{m\beta}. \tag{A.14}$$

Now the attenuation factor, Eq. (A.9), can be calculated by integrating over all detunings (velocities) and over the path of length L giving

$$a = -L \int_{-\infty}^{+\infty} n(\delta)\sigma(\delta)d\delta. \tag{A.15}$$

Since the typical atomic line width $\Gamma \sim 10$ MHz is much smaller than the doppler broadening width $\sigma_\delta \sim 1$ GHz, we can approximate $\sigma(\delta)$ with a dirac delta function with the same area

$$\sigma(\delta) \approx \sigma_0 \frac{\Gamma}{2} \pi \delta(\delta) \tag{A.16}$$

so that the integral is easily evaluated and we have

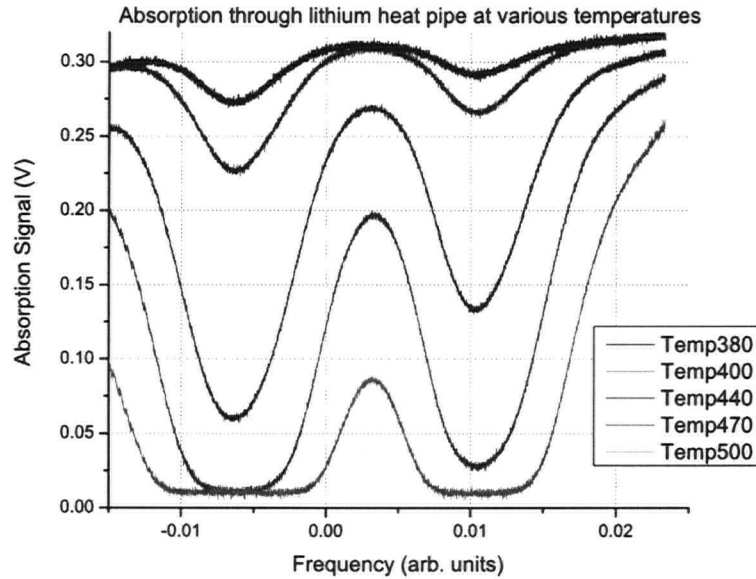$$a = -L \frac{n_0}{\sigma_\delta \sqrt{2\pi}} \sigma_0 \frac{\Gamma}{2} \pi. \tag{A.17}$$

Figure A.1: The following graph shows a series of absorption spectrum measurements for lithium-6 at different heat-pipe temperatures. The D2 line is on the right side, and the D1 line is on the left side. We can clearly see the broadening of spectra as we increase the temperature. Also, absorption increases since optical density increases with temperature, and ultimately we see the saturation effect due to very high optical density disabling any light to come out of the cell. (Note: the temperature value noted here might not be the actual temperature of lithium atoms).

It is worthwhile to observe the following three things:
1. $\sigma_\delta \sim \propto 1/\lambda$ The smaller the wavelength, the greater the effect of doppler broadening.
2. $\sigma_\delta \sim \propto \sqrt{T}$ At higher temperatures, the effect due to doppler broadening is more pronounced.
3. $\sigma_\delta \sim \propto 1/m$ The smaller the mass of the atom, the wider the doppler profile.

All these three are responsible for much larger Doppler broadening of lithium spectrum (around 6GHz) compared to Rb spectrum (around 1GHz).

To get rid of Doppler broadening, we simply use saturated absorption spectroscopy. Details of the scheme are given in chapter 3 of the thesis.

A.4 Pressure broadening

The atom at resonance also interacts with the background particles, and this also affects its spectrum in a complicated way. The theoretical model for this interaction deals with collisions between the atoms and other particles- hence short-range interactions, and how they would affect the unperturbed wave-packet traveling in space. If the collisions in our atomic sample are such that the average time between collisions τ_c is shorter than the excited state lifetime, τ, we can think of these excitations as small square waves in time. Fourier analysis of this gives us a standard Fraunhofer diffraction pattern. However, since this square wave is not periodic, the secondary maxima get smeared out, and we are left with a single, central peak in frequency domain. The rigorous theoretical treatment of this picture is similar to that of natural line-width but the lifetime now is replaced by $\Gamma + \tau_c/2$. See [52] for details. In a simple treatment, the homogeneous width of a transition whose natural width is Γ can be expressed as [38]:

$$\Delta\omega_p = \Gamma + \frac{2}{\tau_c} = \Gamma + 2n_0\sigma\bar{v} \tag{A.18}$$

where σ is again the collision cross-section, and $\bar{v}$ is the mean relative velocity. We calculated the pressure broadening of lithium at 475 ^0C, 2 torr of pressure to be around 4 MHz. That is why the heat-pipe is pumped down in order to reduce the pressure, and hence collisional broadening such that the dominant broadening mechanism is the natural line width.

A.5 Power broadening

For a detailed quantum-mechanical treatment of the problem, refer to chapter 7 of [54]. We start with equation A.9. Here we note that the absorption coefficient has two expressions that are a function of frequency, I and σ, their frequency dependence given by Equation A.10 and Equation A.11 respectively. Substituting those expressions and simplifying, we are left with

$$a = N\sigma_0 \frac{\Gamma^2/4}{(\omega - \omega_0)^2 + \frac{1}{4}\Gamma^2(1 + I/I_s)} \tag{A.19}$$

This expression has a Lorentzian line-shape with a full width at half maxima of

$$\Delta\omega = \Gamma(1 + \frac{I}{I_s})^{1/2} \tag{A.20}$$

We can clearly see that this line-width depends on the intensity of the incoming beam. This effect is called power broadening. It occurs because saturation reduces the absorption near the resonance while absorption changes little far from resonance.

A.6 Transit time broadening

This has to do with the fact that in the transverse dimension, the beams are not uniform or infinitely wide. The atom whizzing in the transverse direction sees the laser beam for a finite amount of time, lets say $\tau_{transit} = \frac{w}{v_0}$ where w is the beam waist, and v_0 is the average velocity of the thermal distribution. This corresponds to a width

$$\Gamma_{transit} = \frac{1}{2\pi\tau_{transit}} \tag{A.21}$$

For normal spectroscopy parameters used in our lab, this broadening is much less than a MHz (for example its around 500 kHz for lithium heat pipe spectroscopy parameters), and hence not of much concern.

A.7 Laser line-width

In all these calculations, we have been assuming that the laser has a well defined frequency of ω. However, in spite of frequency locking mechanism, that is not the case. As shown in the measurements done by beating two locked lasers (see Figure A.2), we can see the master lasers used for the experiment have a line-width of around 3 MHz. This is another source of homogeneous broadening.

A.8 Second order Doppler effect

Saturated absorption spectroscopy eliminates the first order Doppler shift in frequency. However, there is the second order shift in frequency that is attributed to relativity. It depends on v^2, and hence is independent of the direction of velocity. The time dilation corresponding to this effect is approximately given by:

$$\Delta f \approx \frac{v^2}{c^2} f_0 \tag{A.22}$$

Substituting the lithium heat pipe, we get a second order shift of 13 kHz. Although due to the distribution of velocities, this also leads to a broadening mechanism, it can easily be ignored of the atoms are not moving very fast.

A.9 Other mechanisms

There are several other mechanisms that also lead to broadening of atomic spectra, for example inhomogeneities in the electric and magnetic field in the environment. Also, in case of saturated absorption, if the beams are not exactly over-lapping, there is a residual doppler effect. However, the contributions of all these mechanisms are insignificant for our particular experiment and shall not be discussed.
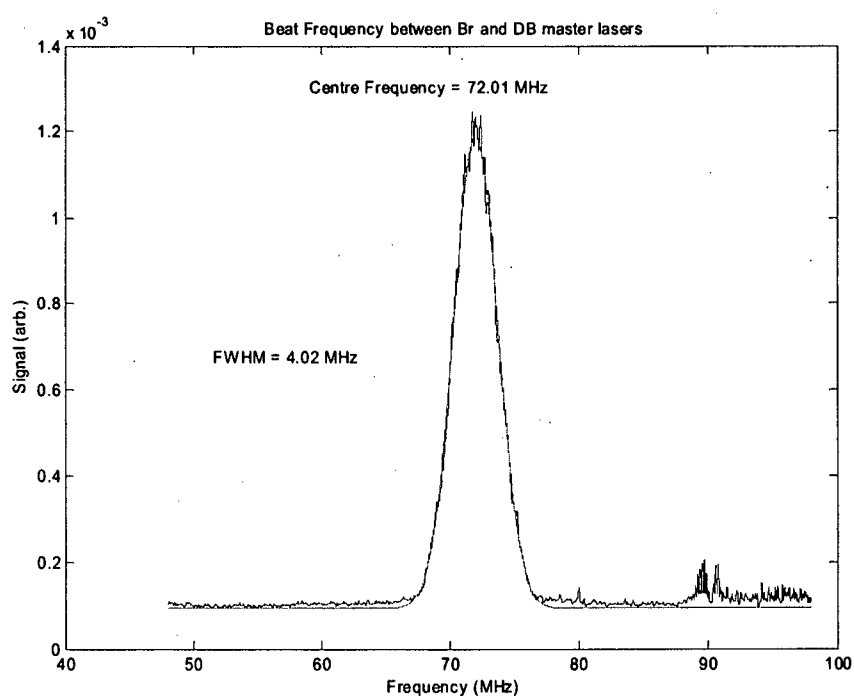
Figure A.2: Line-width of the master lasers as obtained by beating two locked master lasers. Assuming un-correlated errors, the line-width of our lasers is 4.0 MHz/Sqrt(2) = 2.8 MHz.]

Appendix B

Laser System Details

The details of the laser setup are being provided here. This is an extension of chapter 3, that discusses the generation of laser cooling and trapping light. In the following figures, the details of the frequency shifts of various lights and the optical setup details will be explained.

The generation of trapping and re-pump light frequencies via the use of AOMs is being described in the following figures. The zero of frequency corresponds to the trapping or re-pump transition of interest. At the moment, both trapping and re-pump light are set 20 MHz below resonance. However, this is expected to change depending on the efficiency of our recently acquired MOT.

The broken arrows represent the frequency range covered through an AOM. The details of all the AOMs used in the experiment is described in chapter 3, and will not be reproduced here. The black vertical lines represent the transition frequencies for different hyperfine transitions and also cross-over frequencies (represented as X i-f'). The longer grey lines represent the frequency of actual lasers.

The last two figures show the actual table layout of the lithium master table optical setup, and the amplification stage optics on the feshbach table before the MOT. Similar details for the rubidium setup on the master table are not shown because it is very simple, consisting of a saturated absorption setup with an AOM in the pump beam, and a slave injection setup.

On the feshbach table, the EOS crystal between two Glan-Thompson polarizers was initially decided to be used as a fast on-off switch for light, since the DC voltage required to change the polarization of the light going through the EOS crystal can be switched from one state to another very easily. However, the idea is still under consideration and refinement, as the crystals do not perform efficiently mainly due to their inherent spatially inhomogeneous birefringence.
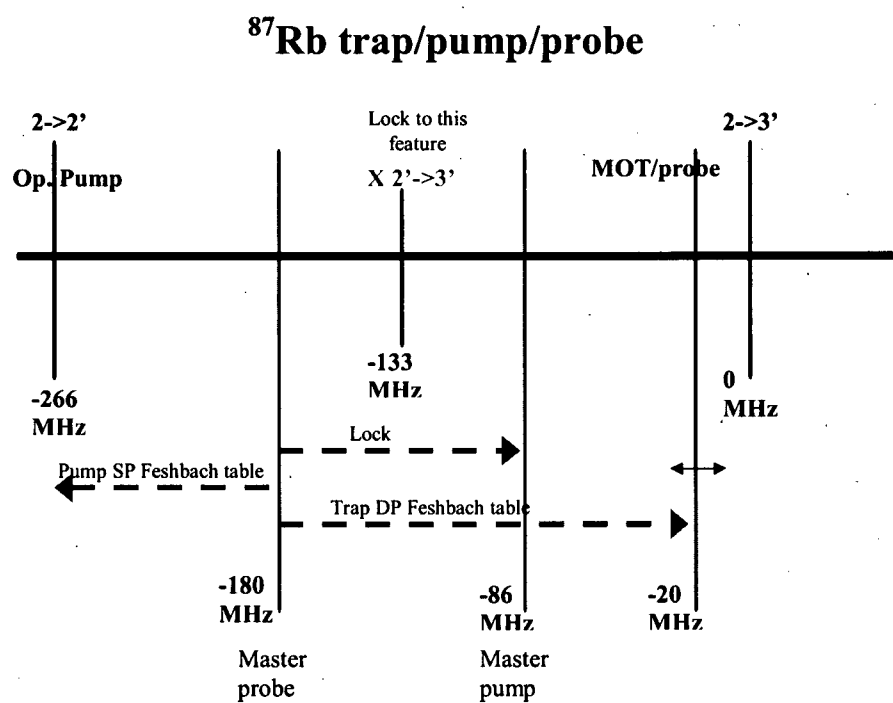
^{87}Rb trap/pump/probe

Figure B.1: Details of the frequency setup to generate light for cycling transition of ^{87}Rb. It also produces light required for optical pumping and imaging measurement.
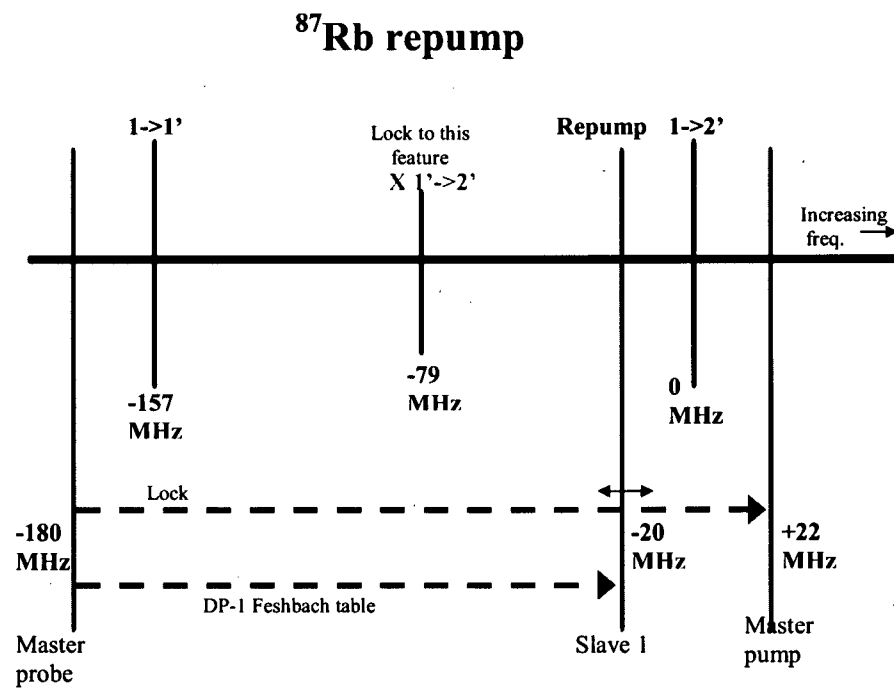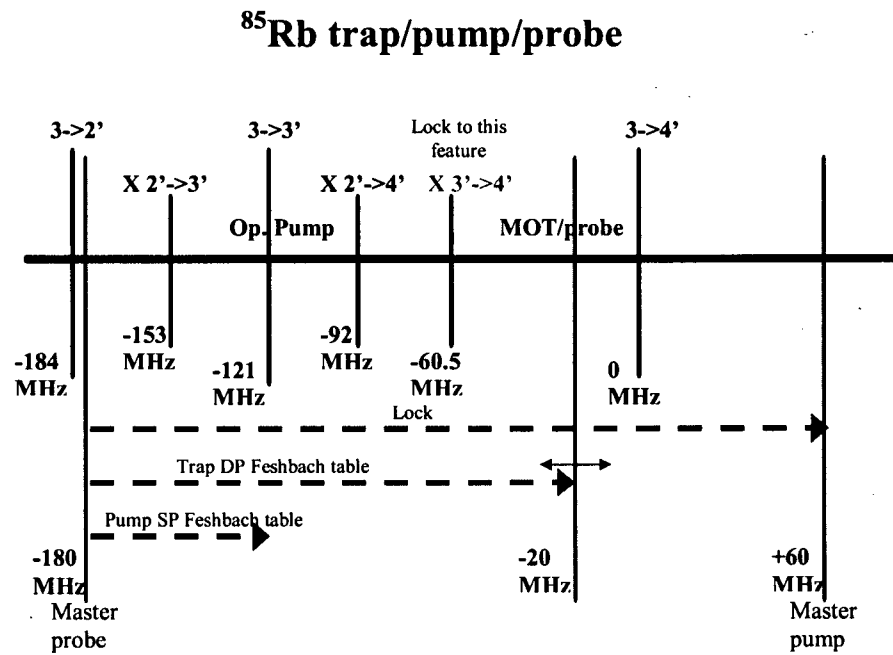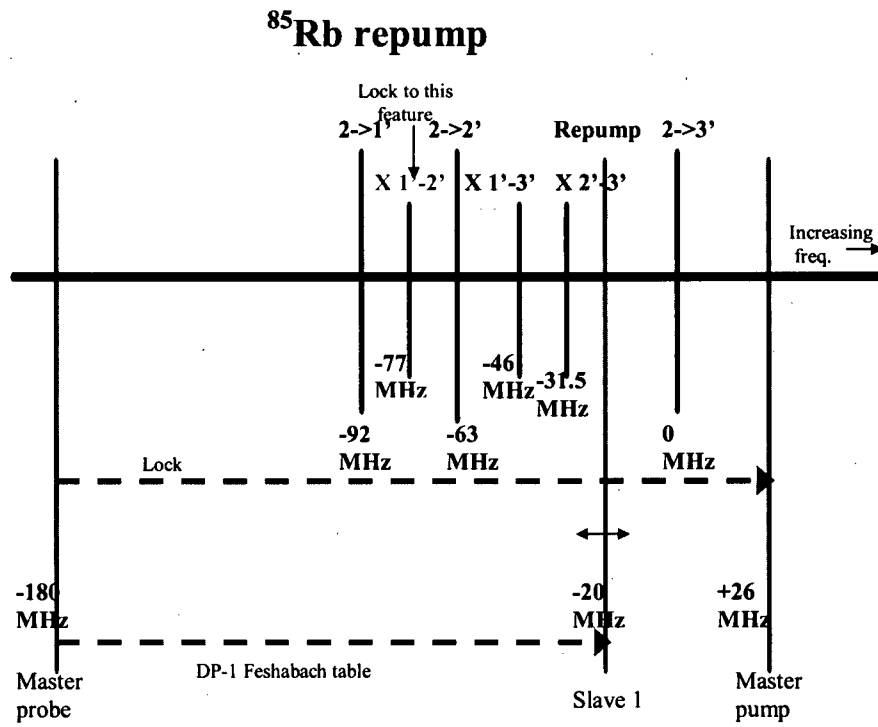
^{87}Rb repump

Figure B.2: Details of the frequency setup to generate light for repump transition of ^{87}Rb.

^{85}Rb trap/pump/probe

Figure B.3: Details of the frequency setup to generate light for cycling transition of ^{85}Rb. It also produces light required for optical pumping and imaging measurement.

^{85}Rb repump

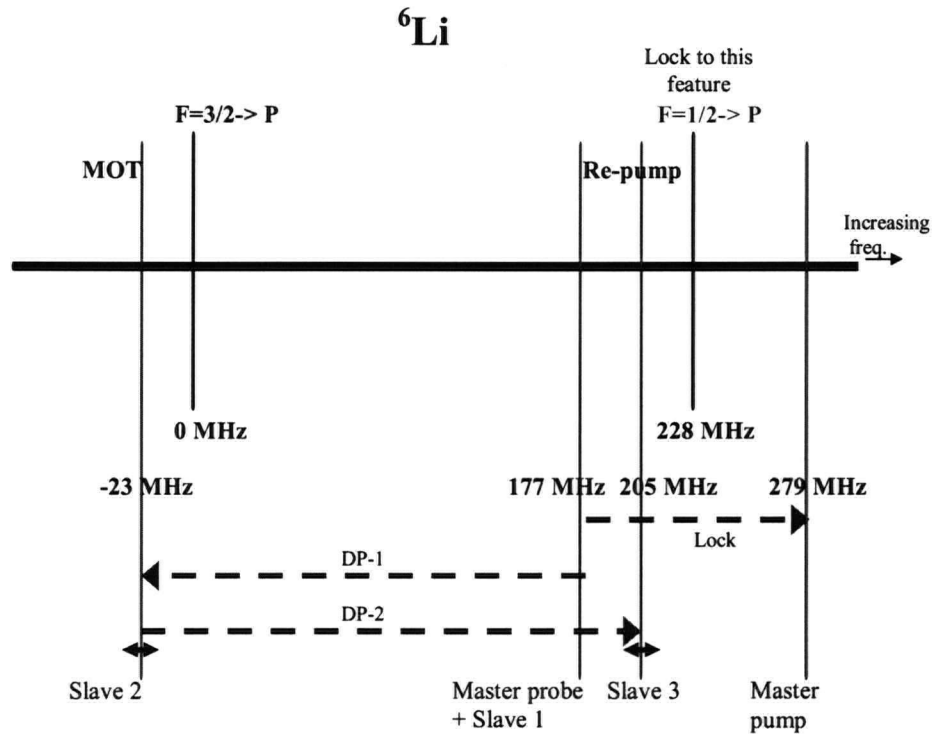Figure B.4: Details of the frequency setup to generate light for re-pump transition of ^{85}Rb MOT.

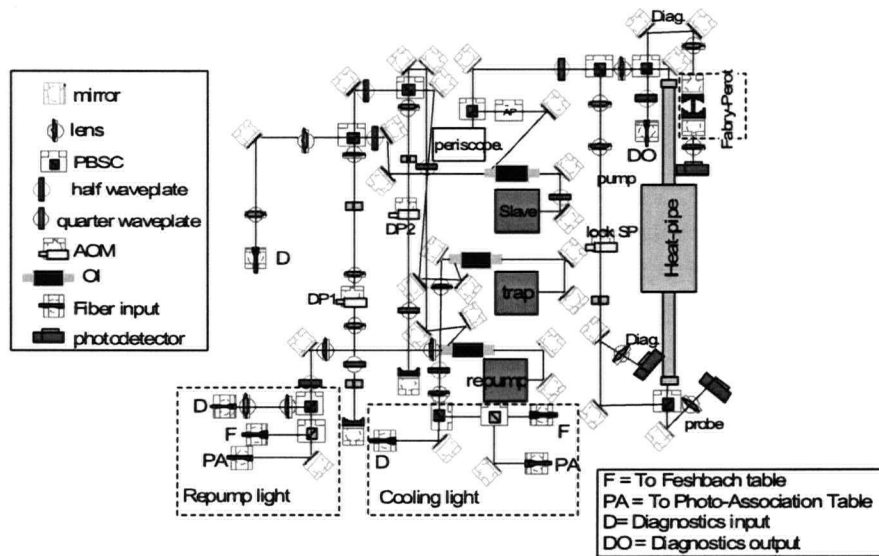Figure B.5: Details of the frequency setup for the lithium MOT.

Figure B.6: Details of the actual optical setup for lithium-6 on the Master table.
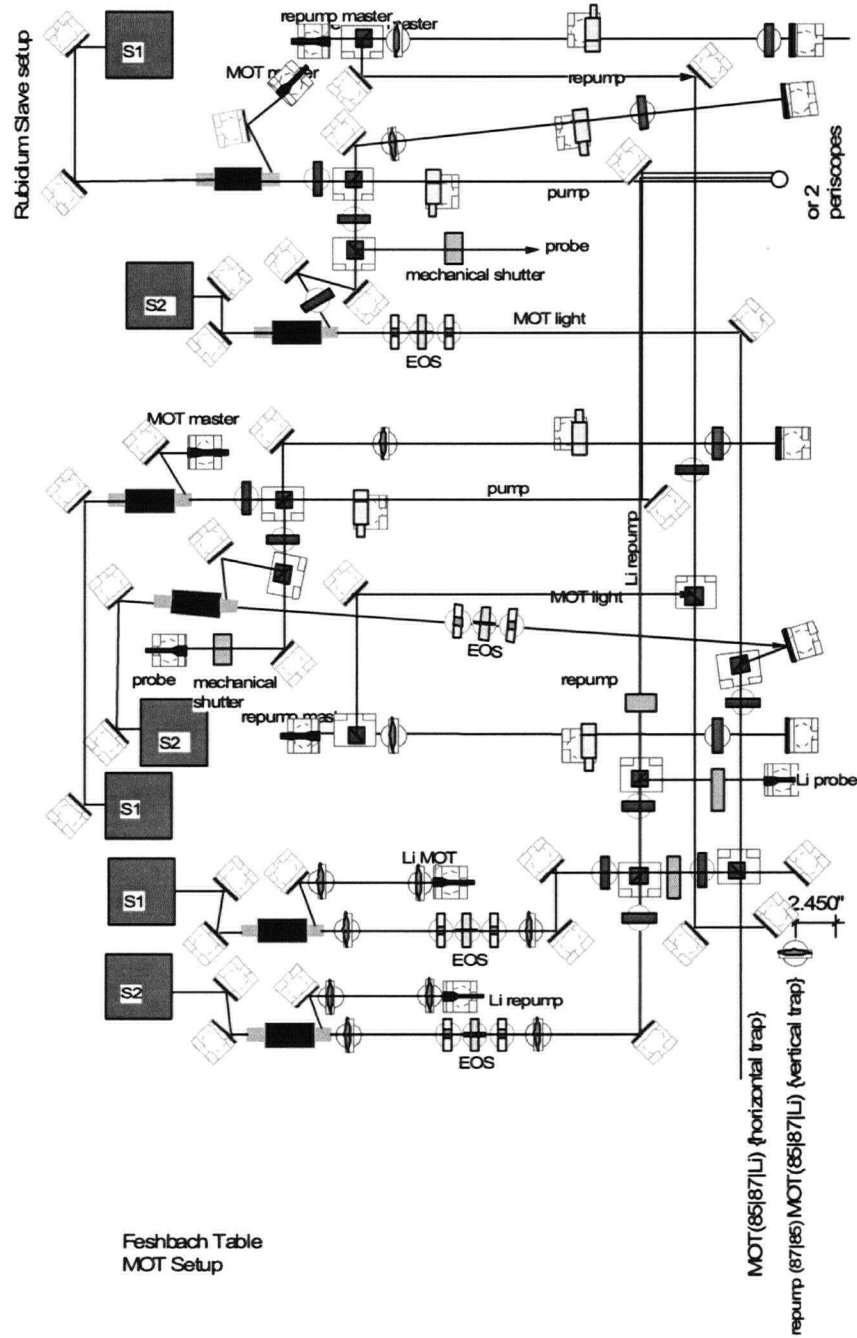
Figure B.7: Details of the amplification stage before the Feshbach table MOT.